Materials Research Bulletin 193 (2026) 113672

Contents lists available at ScienceDirect

Materials Research Bulletin

journal homepage: www.elsevier.com/locate/matresbu

Research Papers

Synthesis, characterization and application of zeolite-A/graphene oxide nanocomposite for ammonia removal from poultry manure: Box-Behnken design optimization

Jimoh Oladejo Tijani [a,j], Muhammad Sani [a], Saheed Mustapha [a,j], Sarah Udenyi Onogwu [b], Hassana Ladio Abubakar [c], Ambali Saka Abdulkareem [d,j], Oluwatosin Kudirat Shittu [e,j], Abdulsalami Sani Kovo [d,j], Titus Chinedu Egbosiuba [f], Alechine Emmanuel Ameh [g,h], Muhammed Muhammed Ndamitso [a,j], Ogunmuyiwa O. Enoch [i], Omar H. Abd-Elkader [k], Hamad A. Al-Lohedan [l], Abdelrahman O. Ezzat [l,*]

[a] Department of Chemistry, Federal University of Technology, PMB 65, Bosso Campus, Minna, Niger State, Nigeria
[b] Department of Chemistry, Joseph Sarwuan Tarka University, PMB 2373, Makurdi, Benue State, Nigeria
[c] Department of Chemistry, Nile University of Nigeria, Abuja, Airport Road, Jabi, Abuja, Nigeria
[d] Department of Chemical Engineering, Federal University of Technology, PMB 65, Gidan Kwano Campus, Minna, Niger State, Nigeria
[e] Department of Biochemistry, Federal University of Technology, PMB 65 Bosso Campus, Minna, Niger State, Nigeria
[f] Department of Engineering Technology and Industrial Distribution, Texas A&M University, College Station, TX 77843, USA
[g] Department of Chemistry, University of the Western Cape, Robert Sobukwe, Rd, Private Bag X17, Bellville 7535, South Africa
[h] School of Geography and Environmental Sciences, University of the Witwatersrand, South Africa
[i] Department of Chemical, Materials and Metallurgical Engineering, Botswana International University of Science and Technology, Private Bag 16, Plot 10071, Palapye, Botswana
[j] Nanotechnology Research Group, Center for Genetic Engineering and Biotechnology, Federal University of Technology, PMB 65, Minna, Niger State, Nigeria
[k] Department of Physics and Astronomy, College of Science, King Saud University, P.O. Box 2455, Riyadh 11451, Saudi Arabia
[l] Surfactants Research Chair, Department of Chemistry, College of Science, King Saud University, P.O. Box 2455, Riyadh 11451, Saudi Arabia

ARTICLE INFO

Keywords:
Box-Behnken design
Adsorption
Ammonia removal
Poultry manure
Zeolite-A/graphene oxide nanocomposite

ABSTRACT

This study developed zeolite-A/graphene oxide (GO) nanocomposite for ammonia removal from poultry manure. Zeolite-A, GO, and the zeolite-A/GO composite were synthesized and characterized using various analytical tools. Physicochemical properties of soil and poultry manure were analyzed, and ammonia reduction was assessed using column adsorption with the nanomaterials. HRSEM images showed zeolite-A as uniform cubic shapes, GO with a layered structure, and the zeolite-A/GO composite as stacked cubic-spherical particles. HRTEM images indicated strong interactions with smaller zeolite-A particles within GO sheets. FTIR analysis showed characteristic peaks for both zeolite-A and GO, indicating retention of both materials' features. N_2 adsorption-desorption analysis revealed surface areas of 15.89 m^2/g for zeolite-A, 19.35 m^2/g for GO, and 69.30 m^2/g for the composite. The response surface methodology (RSM) results indicated that zeolite-A/graphene oxide nanocomposites significantly removed 95% ammonia, with adsorbent dosage being the most influential factor, followed by stirring time, while pH had a non-significant effect. The removal efficiencies of ammonia using the adsorbents were temperature-dependent under the influence of optimum parameters from the RSM results.

1. Introduction

The increasing global concern regarding environmental pollution has necessitated the development of effective strategies for the removal of ammonia from wastewater, particularly from agricultural sources such as poultry manure. Ammonia, a nitrogenous compound, poses significant risks to aquatic ecosystems and human health due to its toxicity and potential to cause eutrophication in water bodies [1]. The

* Corresponding author.
E-mail address: aezzat@ksu.edu.sa (A.O. Ezzat).

https://doi.org/10.1016/j.materresbull.2025.113672
Received 15 February 2025; Received in revised form 19 July 2025; Accepted 20 July 2025
Available online 25 July 2025

treatment of ammonia-laden waste is thus critical, and innovative approaches are being explored to enhance removal efficiency. Moreover, the environmental implications of ammonia removal from poultry manure cannot be overstated. The poultry industry is a significant contributor to ammonia emissions, which can lead to air quality issues and contribute to the formation of particulate matter [2]. Effective ammonia removal not only mitigates these emissions but also enhances the overall sustainability of poultry farming practices. Recent studies have highlighted the detrimental effects of ammonia emissions from poultry manure, as well as contribute to greenhouse gas emissions. Various methods for ammonia removal from poultry manure include adsorption, biological treatment, and chemical processes. Adsorption, particularly using materials like biochar and zeolites, has gained attention due to its efficiency and simplicity [3,4]. This method allows for the effective capture of ammonia, minimizing its volatilization and subsequent environmental impact [5]. Compared to other techniques, adsorption offers advantages such as lower operational costs, ease of regeneration, and reduced complexity in implementation [4]. For instance, researcher by indicates that the incorporation of biochar derived from poultry manure can significantly reduce ammonia emissions, alongside other greenhouse gases, by enhancing the thermophilic phase of composting processes [6]. This finding emphasized the importance of utilizing organic amendments to mitigate ammonia volatilization, thereby improving the overall environmental footprint of poultry farming.

Zeolites are microporous, aluminosilicate minerals that possess unique ion-exchange properties, making them highly effective in adsorbing ammonia from aqueous solutions [7]. Recent studies have demonstrated that the performance of zeolites in ammonia removal can be significantly influenced by various operational parameters, including pH, temperature, and the concentration of ammonia in the wastewater [8,9]. It was observed that higher pH levels enhance the adsorption capacity of zeolites, facilitating the ion exchange process that is crucial for ammonia removal. However, zeolite A exhibits limitations in the removal of ammonia from poultry manure primarily due to its relatively low adsorption capacity and susceptibility to ionic interference in high-salinity environments, which can hinder its effectiveness [10]. Graphene oxide, on the other hand, is a derivative of graphene that exhibits excellent mechanical and chemical properties. Its strong C–C bonds, aromatic structure, abundance of free π electrons, and numerous active sites for surface reactions make graphene oxide a unique material with remarkable mechanical, physical, thermal, and optical characteristics [11,12]. These features make it an ideal candidate for enhancing the performance of zeolite composites. The incorporation of graphene oxide into zeolite matrices can improve the structural integrity and surface area of the composite material, thereby increasing its adsorption capacity for organic and inorganic pollutants [13,14]. Furthermore, this composite approach leverages the high surface area and functional groups of GO to improve the adsorption characteristics of zeolite, thereby increasing ammonia removal efficiency [15]. The use of advanced materials such as zeolite- and graphene oxide nanocomposites presents a promising avenue for enhancing the efficiency of ammonia removal processes.

The optimization of ammonia removal processes using response surface methodology (RSM) is a critical aspect of this research. Response Surface Methodology (RSM) is a statistical technique that enables the evaluation of multiple variables and their interactions, allowing researchers to identify the optimal conditions for ammonia removal [16]. Additionally, RSM helps minimize experimental errors and reduces chemical consumption by decreasing the number of experiments required [17]. By systematically varying parameters such as initial ammonia concentration, pH, and contact time, RSM can help in developing a robust model that predicts the performance of zeolite-A/graphene oxide nanocomposites in real-world applications. The optimization of ammonia removal from poultry manure using zeolite-A/graphene oxide nanocomposites represents a significant advancement in environmental remediation. The unique properties of zeolites, combined with the enhancing effects of graphene oxide, provide a powerful tool for addressing the challenges associated with ammonia pollution. Through the application of response surface methodology, this research aims to establish optimal conditions for ammonia removal, thereby contributing to the development of sustainable practices in the agricultural sector. In this study, zeolite-A/GO nanocomposite was synthesized and characterized, and the ammonia removal in poultry manure was optimized using the prepared nanocomposite at different ratios of zeolite and GO.

2. Materials and methods

2.1. Materials

Analytical grade chemicals with specified percentage purities and manufacturers were utilized for this study. These include potassium tetraoxomanganese (VII) (98%, BDH Chemicals England), sodium hydroxide (97%, Merck), acetylene gas (98.9 %, Anqiu Heng China), sulphuric acid (98 %, BDH Chemicals England). ethanol (96 %, BDH Chemicals England), tetraoxosulphate (VI) acid (98%, BDH Chemicals England), hydrogen chloride (37%, BDH Chemicals England), hydrogen peroxide (85%, BDH Chemicals England), and phosphoric acid (98%, BDH Chemicals England).

2.2. Collection and pre-treatment of kaolin and poultry manure

The raw kaolin was collected from a deposit at Lemu, Gbako Local Government, Niger State, Nigeria. The sample was wet beneficiated as described by Mustapha et al. [18], and the resulting kaolinite was oven-dried at 105 °C in an oven. The beneficiated sample is then stored prior to analysis. Manure was collected in a poultry farm area in Minna Metropolis on the 11th of June, 2023. The manure was carefully scooped using a shovel and stored in a container until when needed

2.3. Synthesis of zeolite A, graphene oxide and nanocomposites

2.3.1. Synthesis of graphene and graphene oxide (GO)

The catalytic vapour deposition (CVD) method was used for the synthesis of graphene particles. A flow of N_2/H_2 gas was introduced into the reactor for 15 min to remove the present oxygen and to reduce the copper oxides on the surface of the sheet. Afterward, acetylene was introduced to the reactor at a constant flow rate of 230 mL/min. The injection of acetylene gas was maintained for 30 min to enable proper growth of graphene, and later, the flow of acetylene gas was stopped. The cooling down was carried out under a nitrogen atmosphere with a ramp of 8°C/min.

A mixture of concentrated H_2SO_4 and H_3PO_4 was prepared in a beaker at a ratio of 3:1. This step helped improve the oxidation efficiency and prevent the overheating of the reaction mixture. Graphene powder was added slowly to the acid mixture while stirring continuously, ensuring that the graphene was completely submerged in the acid. The addition of $KMnO_4$ was done gradually and cautiously to avoid excessive heat generation. The mixture was stirred at 150 rpm for 10 min at 80°C, allowing the oxidation reaction to proceed effectively. After the desired reaction time, the reaction was quenched by adding cold water to the mixture, halting the oxidation process. The resulting mixture was washed thoroughly with 0.2 M H_2SO_4 and H_2O_2. Filtration was used to separate the solid graphene oxide from the liquid. Finally, the graphene oxide was further purified using 0.5 M HCl to remove any metal impurities present in the graphene oxide (see Fig. 1).

2.3.2. Synthesis of zeolite-A

The beneficiated kaolin was calcined at 600 °C for 12 h. The resulting metakaolin was used for the synthesis of zeolite-A. The zeolite-A was synthesized through the hydrothermal route, which is a multiphase

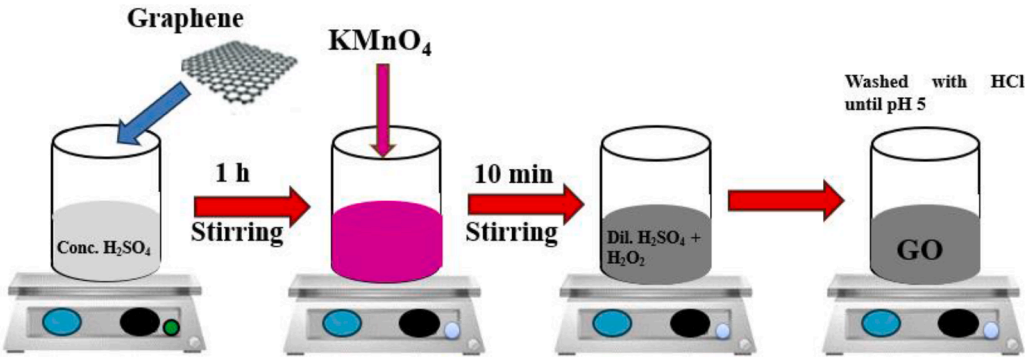

Fig. 1. Pictorial representation of the synthesis of graphene oxide.

reaction–crystallization process. Zeolite-A was prepared by alkali treatment of metakaolin with 5.0 mol/dm^3 aqueous NaOH solution, and $Al_2Si_2O_7$ was considered the formula of the metakaolin. The mixture was maintained under magnetic stirring and heated in a Teflon autoclave at 105 °C for 3 h. The resulting zeolite-A was washed with de-ionized water several times and dried at 110 °C (Fig. 2).

2.3.3. *Synthesis of zeolite-A/graphene oxide*

A known weight of zeolite-A was added to graphene oxide to form weight ratios of zeolite/GO (1:1), (1:2), and (2:1), respectively, were weighed into a 200 cm^3 beaker, dispersed in 100 cm^3 and stirred at 150 rpm for 5 h using a magnetic stirrer. This mixture allowed electrostatic interactions between the surface of zeolite-A and GO. After impregnation, the material was oven-dried at 105 °C to obtain complete dryness. The resultant product was pulverized in a ceramic mortar to achieve uniform particle size and better integration between zeolite-A and GO. The resulting zeolite-A/graphene oxide nanocomposite was collected and further characterized or used in the application.

2.4. *Characterization*

The study characterized GO, zeolite-A, and zeolite-A/GO nanocomposites using several analytical techniques. X-ray diffraction (XRD) was employed to assess graphitization and identify mineral phases in the samples, scanned from 20° to 90° at a 2°/min rate. High-resolution scanning electron microscopy (HRSEM) with energy dispersive spectroscopy (EDS) determined the morphology and elemental composition of nanoparticles. High-resolution transmission electron microscopy (HRTEM) examined sample structure and morphology, with samples prepared on copper grids and imaged at 5 kV. Fourier transform infrared spectroscopy (FTIR) analyzed samples across 400-4000 cm^{-1}, purged with nitrogen during data collection to exclude interference. Brunauer-Emmett-Teller (BET) analysis assessed surface area, pore sizes, and volumes using nitrogen gas after sample degassing at 250 °C for 3 h.

2.5. *Determination and removal of ammonia removal using nanoadsorbent*

The efficiency of nanomaterials in removing NH_3 was performed using response surface methodology. They varied stirring time (30 to 60 min), pH (3 to 12), and dosage (1 to 5 g) (as detailed in Table 1) using Design Expert 13.0 software. Zeolite-A/GO in ratios of 1:1, 1:2, and 2:1 was tested across 17 experiments (per Table 1). Initially, manure was weighed into batch adsorption, and its ammonia content was quantified using the gas detector (Model S316). After blending with nanocomposites, ammonia levels were reassessed to gauge removal efficacy.

2.6. *Effect of temperature*

The effect of temperature on the adsorption of NH_3 using zeolite A and the composites of zeolite A/GO was performed at different ranges of 30 to 80 °C, and optimum dosage of adsorbent, pH, and stirring time was obtained from the RSM. The Flory-Huggins model and Gibb's free energy, as illustrated in Equ. 1 and 2, respectively, were explored for the experimental data in the study.

Table 1
Independent variables and their coded degree for removal of ammonia.

Independent Variables	Symbols	Range and level		
		Low (-1)	Middle (0)	High (+1)
pH	A	3	7.5	12
Stirring time (min)	B	30	45	60
Dosage (g)	C	1	3	5

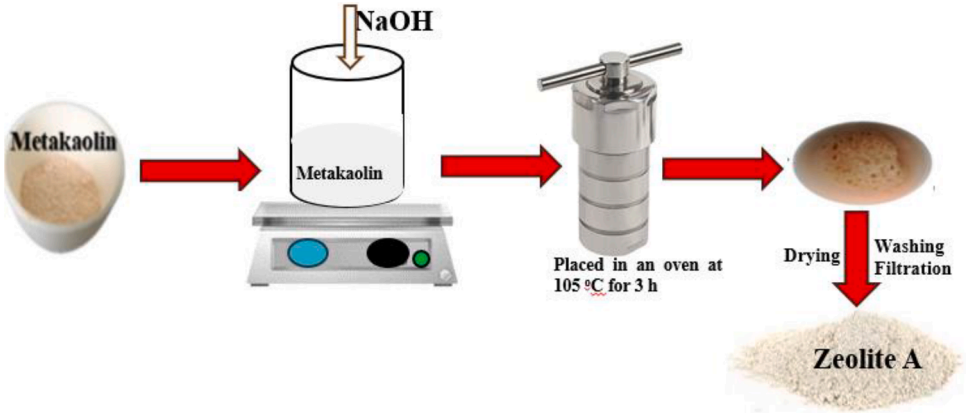

Fig. 2. Pictorial representation of the synthesis of zeolite A.

$$\log \frac{\theta}{C_e} = \log K_{FH} + n_{FH} \log (1-\theta) \quad (1)$$

$$\Delta G = -RT \ln K_{TH} \quad (2)$$

where $\theta = \left(1 - \frac{C_e}{C_o}\right)$, the Flory-Huggin's equilibrium constants are K_{FH} and n_{FH}, ΔG is Gibb's free energy, R is the gas constant, and T is the absolute temperature.

3. Results and discussion

3.1. Characterisation of zeolite-A, GO and zeolite-A/GO

3.1.1. HRSEM/EDX of zeolite-A, GO and zeolite-A/GO

The morphologies of zeolite-A, GO, and the zeolite-A/GO composite were analyzed using HRSEM, and the results are presented in Fig. 3. In Fig. 3(a), the image reveals that the pristine zeolite-A crystals exhibited uniform cubic shapes, consistent with the findings reported by Wang et al. [19]. Furthermore, Ren et al. [20] found that zeolite-A synthesized from coal fly ash had a well-defined cubic shape. Morales et al. [21] confirmed the uniform cubic morphology of zeolite-A synthesized from rice husk ash. Zeolite-A, with its well-defined cubic crystal morphology, suggests an increased nucleation rate in the synthesis system and an elevated rate of polymerization between silicate ions and aluminate ions, resulting in the formation of orthorhombic within the synthetic system.

The micrograph of GO, shown in Fig. 3(b), depicts a layered structure with multiple stacked sheets, indicating a highly rough surface attributed to the presence of stacked graphene layers and graphitic material. The combination of zeolite-A and GO, illustrated in Fig. 3(c), exhibits a stacked structure of spherical particles, likely resulting from the self-assembly between GO and zeolite-A. The existence of Van der Waals and hydrogen bonding forces, as suggested by Shi et al. [22], contributed to the formation of this composite.

Zeolites are primarily aluminosilicates, containing Si and Al, while GO contains carbon (C) and oxygen (O). This allows the potential formation of GO covalent bonding with the aluminosilicate framework of zeolite-A, ionic interactions between the negatively charged oxygen functional groups on GO (e.g., carboxyl, hydroxyl), and exchangeable cations (e.g., Na^+, Al^{3+}) and GO forming hydrogen bonds with the hydroxyl groups on the surface of zeolite-A. The presence of Si and Al in zeolite-A, as well as C and O in graphene oxide (GO), has been confirmed in previous literature [23]. This supports the successful formation of a nanocomposite between zeolite-A and GO, as indicated by the presence of C, O, Al, Na, and Si [23]. Fig. 4 shows that the elemental mapping of the nanocomposite mainly consists of four elements: carbon, oxygen, aluminium, and silicon.

3.1.2. HRTEM/SAED of zeolite-A, graphene oxide and zeolite-A/graphene oxide

The HRTEM images in Fig. 5 depict zeolite-A, GO, and the zeolite-A/GO composite. Zeolite-A particles typically exhibit a cubic or pseudo-cubic shape, as shown in Fig. 5(a). Zeolite-A possesses a porous structure with interconnected channels and cavities, identifiable by regions with varying electron density, which appear darker in the HRTEM image. Zeolite-A possesses a porous structure with interconnected channels and cavities, which is consistent with previous findings as described by Gao et al. [24]. The SAED image reveals that zeolite-A contains both amorphous regions, characterized by a regular arrangement of dots or fringes, and crystalline regions delineating the framework boundaries. The mosaic structure of zeolite-A, as revealed by Qin et al. [25], is characterized by segmented crystals with nanometer-sized domains and low-angle boundaries. This is consistent with the presence of dots or fringes and crystalline regions delineating framework boundaries, as observed in the SAED image.

Fig. 5(b) presents a HRTEM image illustrating a large folded sheet of graphene oxide. The electron diffraction rings obtained from SAED measurements in Fig. 5(b) show "d" spacings of approximately 0.12 nm and 0.21 nm, corresponding to the "d" spacings in graphene. This suggests the presence of graphitic regions within the graphene oxide. Fig. 5 (c) reveals a representative HRTEM image of the synthesized zeolite-A/GO composite. It is evident that the as-synthesized zeolite-A/GO composite exhibits a flake-like shape consistent with the SEM results. Furthermore, dark spots, representing zeolite-A cubic particles, are embedded in the GO sheets. This observation suggests the potential for strong interactions between zeolite-A particles and GO sheets, resulting

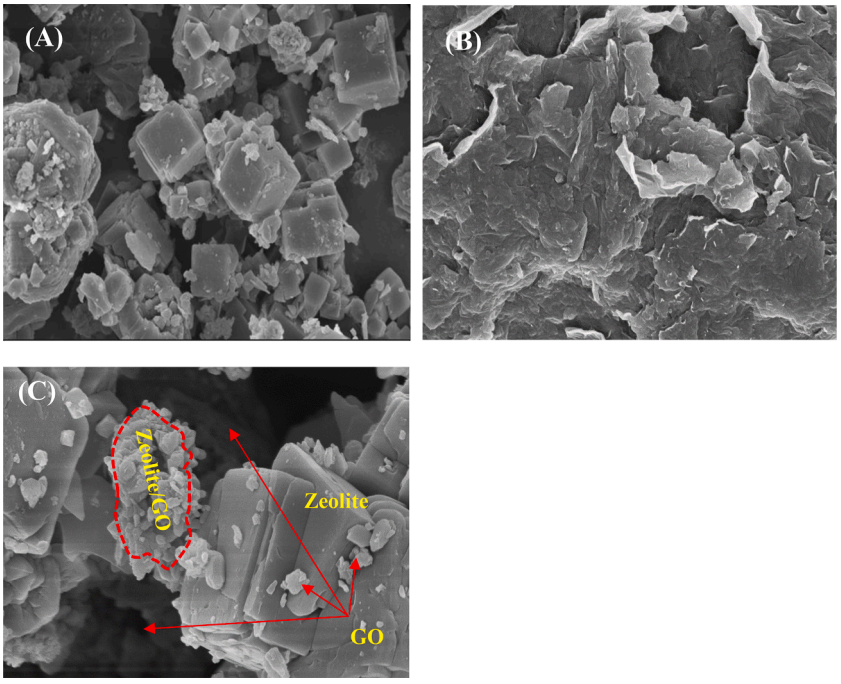

Fig. 3. HRSEM images of (a) zeolite-A (b) GO and (c) zeolite-A/GO nanocomposite.

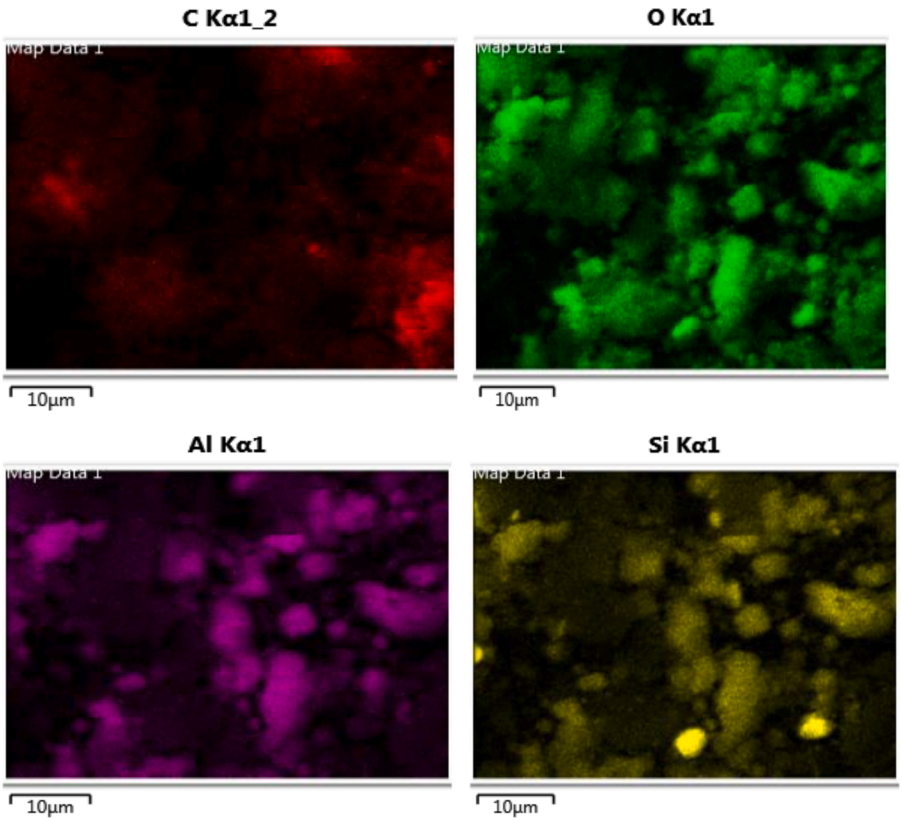

Fig. 4. Elemental mapping of the nanocomposite.

in homogeneously ordered structures in the composite [26]. Thus further confirming that the zeolite in the composite differs from the original zeolite-A due to the formation of new chemical bonds between zeolite A and GO.

3.1.3. *XRD of zeolite-A, graphene oxide and zeolite-A/graphene oxide*

The XRD patterns for zeolite-A, GO, and the zeolite-A/GO composite are displayed in Fig. 6. In Fig. 6(a), the XRD pattern of zeolite-A exhibited a crystalline aluminosilicate material. Its XRD peaks typically appear at 2θ values around 9.7°, 11.6°, 15.2°, 22.5°, 23.1°, 26.6°, 28.1° and 31.9°. These peaks correspond to the characteristic crystallographic planes of the zeolite-A structure, such as (100), (002), (101), (004), (210), (211), (220), and (820), respectively. (JCPDS file No: 73-23400. The XRD peak observed at 29° in the spectrum of graphene oxide typically indicates the interlayer spacing between the graphene layers (Fig. 6b). This peak corresponds to the (002) reflection plane of graphene oxide, which is the interlayer spacing of the oxygen-containing functional groups within the graphene oxide structure. The broadening of this peak indicates the presence of disorder and the heterogeneous distribution of functional groups on the graphene oxide sheets [27]. The XRD pattern of the zeolite-A/GO composite exhibits diffraction peaks from both zeolite-A and GO, indicating significant interaction between the two samples (Fig. 6c). The intensity peak of carbon in the nanocomposite is reduced compared to the peak intensity of carbon in GO as a result of interaction between the graphene oxide sheets and the zeolite framework. This interaction can lead to changes in the crystal lattice parameters and local atomic arrangements, resulting in shifts or modifications in the intensity peaks compared to pure zeolite-A. Elkartehi et al. [28] reported that the successful growth of Zn-Fe layered double hydroxide (LDH) crystals on zeolite particles, as observed in the XRD pattern of zeolite/LDH composites, supports the idea of interactions between different phases in composite materials affecting XRD patterns. This suggests that GO sheets within the composite may have formed strong interactions with the zeolite during the synthesis process. Li et al. [23] found that GO facilitated the solvent-free synthesis of well-dispersed, faceted zeolite-A crystals, suggesting a strong interaction between the two materials. This was further confirmed by Li et al. [29], who observed the growth of zeolite-A crystals with GO nanosheets, indicating a strong bond between the two. Given that GO contains functional groups such as hydroxyl, carboxylic, and epoxy groups, it is likely that the presence of GO facilitates the formation of hydrogen bonds between GO and zeolite, resulting in a homogeneous combination of the composite.

3.1.4. *FTIR spectra of zeolite-A, graphene oxide and zeolite-A/graphene oxide*

FTIR analysis reveals distinctive peaks at specific wavenumbers, indicating various functional groups and structural characteristics, as shown in Fig. 7. The FTIR spectrum of zeolite-A (Fig. 7a) displays several characteristic peaks at specific wavenumbers. At 1640 cm^{-1}, a prominent peak suggests the presence of water molecules adsorbed on the zeolite surface. This absorption band corresponds to the bending vibration of water molecules, indicating the presence of physically adsorbed water [30]. The peak at 1390 cm^{-1} is attributed to the symmetric stretching vibration of Si-O bonds within the zeolite-A framework. This peak is a signature of the crystalline structure of zeolite A, indicating the presence of silicon and oxygen atoms in the lattice [31]. The band observed at 983 cm^{-1} corresponds to the asymmetric stretching vibration of Si-O bonds. This peak further confirms the presence of the zeolite framework, indicating the structural integrity of the material. At 701 cm^{-1}, a peak indicates the presence of Al-O-Si bending vibrations, suggesting the presence of aluminum atoms in the zeolite framework [32]. This peak is indicative of the framework's aluminum content, which can influence the catalytic and adsorption properties of the zeolite-A. The peak at 570 cm^{-1} is attributed to the bending vibrations of the T-O-T units (where T represents Si or Al) within the zeolite framework [33]. This peak

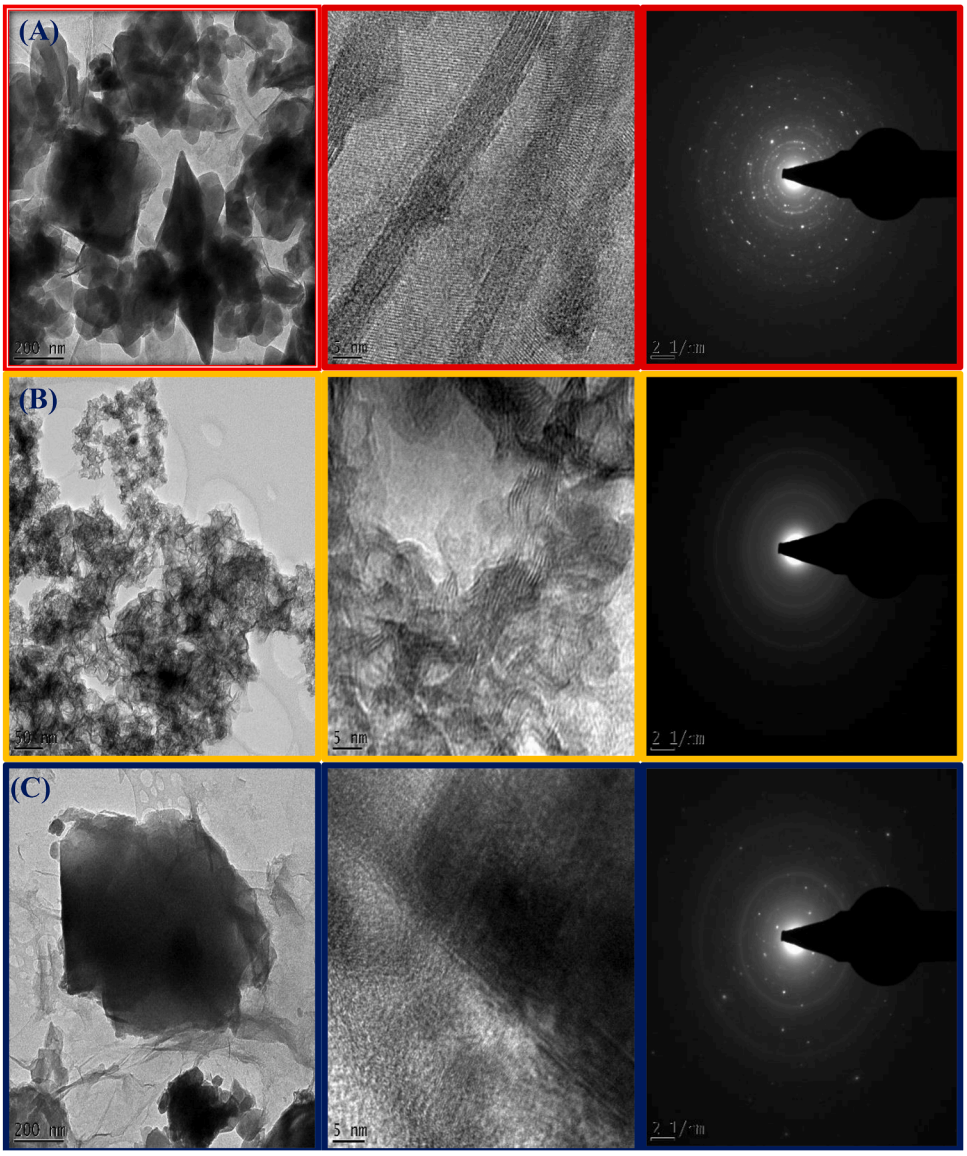

Fig. 5. Low and high magnification HRTEM and SAED images of (a) zeolite-A (b) GO and (c) zeolite-A/GO nanocomposite.

provides additional confirmation of the presence and integrity of the zeolite structure. The peak observed at 440 cm^{-1} is typically associated with the presence of framework vibrations in zeolite materials [34]. This peak further confirms the crystalline nature of zeolite-A and indicates the structural stability of the material.

For graphene oxide (Fig. 7b), the peak at 3520 cm^{-1} corresponds to the stretching vibration of hydroxyl (OH) groups. This suggests the presence of hydroxyl functionalities due to oxidation of graphene, which is common in graphene oxide. At 1658 cm^{-1}, this peak is attributed to the stretching vibration of the carbonyl (C=O) groups [35]. The presence of carbonyl groups signifies the oxidation process of graphene and the introduction of carboxyl and epoxy groups. The peak at 1618 cm^{-1} represents the C=C stretching vibration, which is indicative of the presence of aromatic carbon bonds in graphene oxide. The peak is consistent with the presence of sp^2C–H and sp^3C–H in graphene nano-ribbons [36]. This is further supported by the presence of hydrogen adsorbed on graphene, which exhibits distinct C–H stretching vibrations [37]. The aromaticity of graphene, with two π-electrons delocalized over each hexagon ring, also aligns with the presence of aromatic carbon bonds [38]. The relaxation of the C-H stretch mode in graphene, with a short lifetime, further supports the presence of these bonds [39]. Despite the oxidation, the residual aromatic structure of graphene is retained. The peak observed at 1103 cm^{-1} corresponds to the stretching vibration of epoxy (C-O) groups. Epoxy groups are formed during the oxidation process and contribute to the functionalization of graphene oxide. The peaks at 622 cm^{-1} and 588 cm^{-1} are attributed to the out-of-plane bending vibrations of oxygen-containing functional groups, such as epoxy and hydroxyl groups. These peaks further confirm the presence of these functional groups within the graphene oxide structure.

The FTIR spectrum of zeolite-A/graphene oxide composite (Fig. 7c), specific wavenumbers such as 983 cm^{-1}, 660 cm^{-1}, 546 cm^{-1}, and 450 cm^{-1} are particularly noteworthy due to their indicative features. At 983 cm^{-1}, a characteristic peak is often observed in FTIR spectra of zeolite-A, corresponding to the stretching vibration of Si-O bonds in the zeolite-A framework. This peak signifies the presence of silicon-oxygen bonds within the zeolite-A structure, indicating the integrity of the zeolite lattice in the composite. The peak at 660 cm^{-1} typically corresponds to the bending vibration of Si-O-Si bonds in zeolite frameworks. The presence of this peak suggests the presence of silicon atoms bridging oxygen atoms within the zeolite structure, further supporting the structural integrity of the zeolite-A component in the composite material [40]. At 546 cm^{-1}, a peak may be attributed to the stretching vibration of

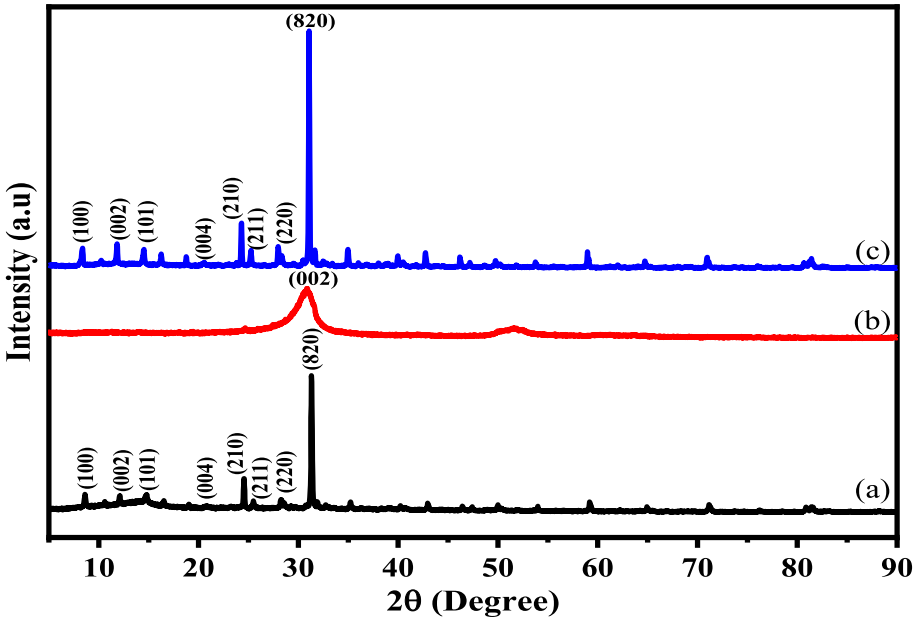

Fig. 6. XRD patterns of (a) Zeolite-A (b) GO and (c) Zeolite-A/GO nanocomposite.

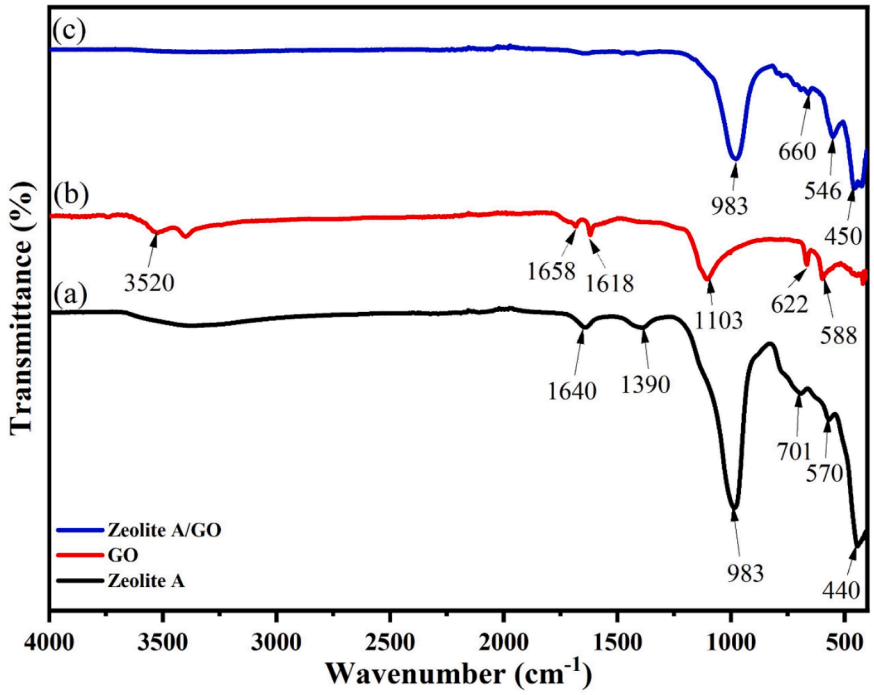

Fig. 7. FTIR spectra of (a) Zeolite-A, (b) GO and (c) Zeolite-A/GO nanocomposite.

C-O bonds, which can arise from the presence of oxygen-containing functional groups, such as hydroxyl (-OH) or carbonyl (C=O) groups [41]. This peak could be indicative of the presence of functionalized graphene oxide within the composite, as graphene oxide often contains oxygen-containing groups on its surface. The peak at 450 cm^{-1} may be associated with the bending vibration of O-Si-O bonds in the zeolite framework [42]. This peak reinforces the presence of silicon-oxygen bonds within the zeolite-A lattice, further confirming the presence of the zeolite-A component in the composite material.

3.1.5. BET of zeolite-A, graphene oxide and zeolite-A/graphene oxide

Fig. 8(a–c) displays the textural characteristics of zeolite-A, graphene oxide, and the zeolite-A/GO composite, as determined from N_2 adsorption-desorption measurements. The specific surface areas for zeolite-A, GO, and the zeolite-A/GO composite are 15.89 m^2/g, 19.35 m^2/g, and 69.30 m^2/g, respectively. Zeolite-A (see Fig. 8a) exhibits minimal nitrogen adsorption at low relative pressure due to its mesoporous nature. In contrast, as depicted in Fig. 8(b), GO exhibits low nitrogen sorption due to its nonporous structure, while the zeolite-A/GO composite (see Fig. 8c) presents a type I isotherm with an entirely irreversible adsorption and desorption branch, signifying the presence of significant mesopores within the composite. Notably, it displays a substantial hysteresis loop between the adsorption and desorption curves, implying the existence of mesoporous gaps between the sample

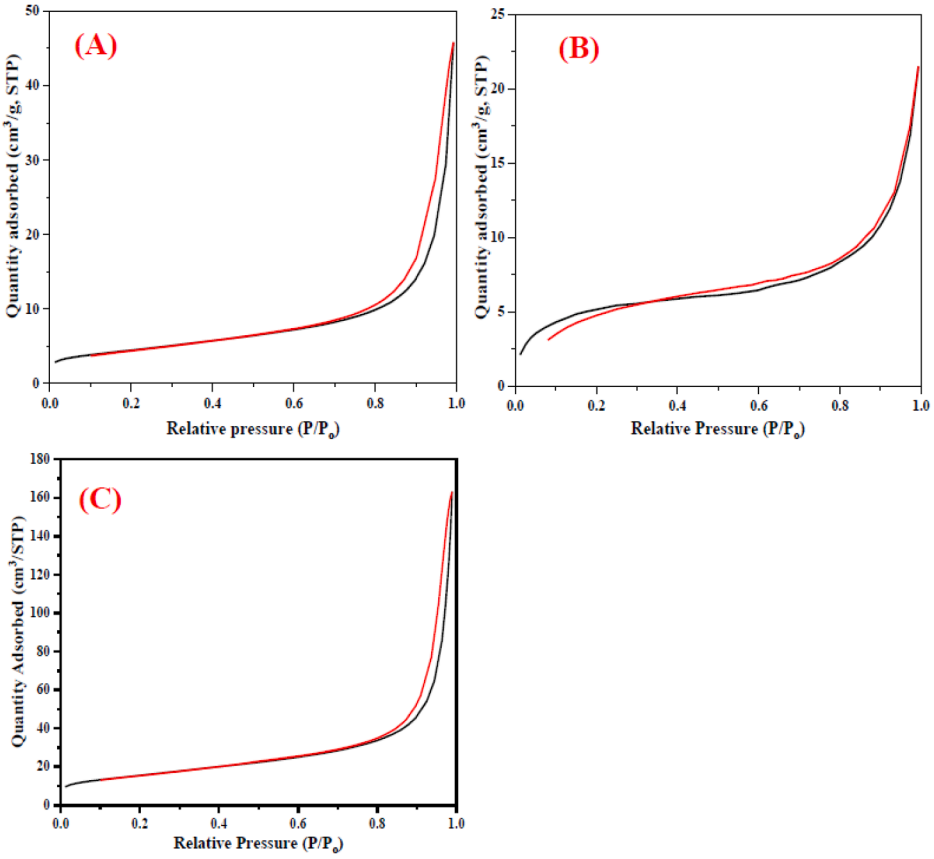

Fig. 8. N_2 adsorption-desorption curves of (a) zeolite-A (b) GO and (c) zeolite-A/GO nanocomposite.

particles, a feature distinct from both GO and zeolite-A. The presence of mesoporous gaps in a sample, distinct from both GO and zeolite-A, is indicated by a substantial hysteresis loop between the adsorption and desorption curves [43]. The role of micropore structure and ion exchange treatment in the occurrence of low-pressure hysteresis loops in natural zeolites is also highlighted [44]. Additionally, the presence of micropores associated with mesopores is indicated by an increase in adsorbate volume in the low P/P_o region in nitrogen adsorption-desorption isotherms [45].

Furthermore, as summarized in Table 2, the textural properties of the zeolite A/GO composite can be tailored by regulating the GO content in the composites. In general, in comparison to pure zeolite-A and GO, the surface area, pore volume, and pore size of zeolite A/GO experience a notable increase. This increase in surface area can be attributed to a synergistic effect characterized by strong interactions between zeolite-A and GO, resulting in the development of new porosities within the *in-situ* synthesized composite. Silva et al. [46] demonstrated a significant increase in surface area and a decrease in pore diameter in zeolite-A particles coated with GO, indicating a synergistic effect between the two materials. This was supported by Chaturvedi and Kundu [47], who found that the rough surface of zeolite combined with the oxygen-containing functional groups of GO facilitates the even dispersion of metal nanoparticles, leading to an increased active surface area. This synergistic effect not only facilitates the creation of new porosity between zeolite-A and GO units but also encourages the formation of intricate "lace-like" structures where zeolite crystals are embedded within GO sheets.

Table 2
Summary of the BET results of zeolite A, GO, and zeolite A/GO.

Sample	Surface area (m^2/g)	Pore size (nm)	Pore volume (cc/g)
Zeolite-A	15.88	16.12	0.0734
GO	19.35	5.58	0.0327
Zeolite-A/GO	69.30	3.21	0.00598

3.2. *Physicochemical parameters of poultry manure*

The physicochemical analysis results of poultry manure samples in Table 3 indicate the composition and its quality.

The moisture content of the samples is notably high, with a mean value of 50.02%, exceeding the recommended range of 20% to 35%, according to the World Health Organization [48]. This high moisture content can affect the handling and storage of the waste material, potentially leading to microbial growth and odor. Total solids (TS) in the samples are also elevated at 50.04%, surpassing the desirable range of 20% to 25%. This high TS value may indicate a concentration of organic and inorganic substances in the poultry manure, potentially affecting its suitability for certain disposal or treatment methods. The research by Falodun and Egharevba [49] on onion growth with poultry manure application corroborates the importance of manure composition, including TS, for plant nutrient uptake and yield. The total organic nitrogen (TON) content is slightly elevated at 6.19%, exceeding the recommended limit of below 5%. Elevated TON levels may indicate the presence of nitrogen-rich compounds, which could contribute to environmental pollution if not properly managed. Total organic carbon (TOC) content is significantly elevated at 28.33%, exceeding the recommended limit of below 5%. This suggests a high concentration of organic carbon compounds in the waste, which could impact soil fertility and microbial activity if the waste is used as a fertilizer or soil amendment. Total organic matter (TOM) content is also elevated at 47.76%, surpassing the recommended limit of below 40%. High TOM levels may indicate a significant dosage of organic material in poultry manure, potentially influencing its decomposition rate and nutrient

Table 3
Physicochemical properties of poultry manure samples.

Parameter	A	B1	B2	B3	Mean value	Standard WHO [48]
Moisture (%)	35.86	56.14	52.33	55.76	50.02 ± 4.8	Below 20% to 35%
TS (%)	64.40	43.86	47.67	44.24	50.04 ± 4.86	Above 20-25
TON (%)	7.72	5.65	5.90	5.48	6.19 ± 0.52	Below 5
TOC (%)	32.34	28.00	26.74	26.25	28.33 ± 1.39	Below 5
TOM (%)	52.62	48.16	45.11	45.15	47.76 ± 1.77	Below 40
pH	5.86	6.28	6.16	6.18	6.12 ± 0.09	6 to 8
EC (μS/cm)	2978	3164	3270	3195	3151.75 ± 62.04	Below 4,000
TOP (mg/kg)	26.44	22.38	30.46	28.38	26.92 ± 1.72	Below 500
Ca (cmol/kg)	5.35	3.98	3.85	3.85	4.26 ± 0.37	Below 20
Mg (cmol/kg)	3.88	3.50	3.50	3.35	3.56 ± 0.11	Below 10
K (cmol/kg)	4.15	3.83	3.90	3.10	3.75 ± 0.23	Below 10
Na (cmol/kg)	1.85	1.76	1.82	1.80	1.81 ± 0.02	Below 5
NH_4 (mg/L)	2566	2144	2310	1955	2243.75 ± 129.6	Below 100
Fe (mg/kg)	7.84	10.42	8.33	8.88	8.87 ± 0.56	Below 500
Cu (mg/kg)	1.18	1.75	1.54	1.66	1.53 ± 0.13	Below 100
Zn (mg/kg)	3.20	3.56	3.72	3.48	3.49 ± 0.11	Below 500

Keys: TS: Total Solid, TOB = Total Organic Nitrogen, TOC = Total Organic Carbon, TOM = Total Organic Matter, EC = Electrical Conductivity (measure of the "total salts" concentration) TOP = Total Organic Phosphorus, A, B1, B2 and B3: Samples from different sites.

release when applied to soil. Research by He et al. [50] supports this by discussing how long-term chemical fertilizer application can reduce soil fertility and hinder soil organic carbon (SOC) accumulation. Rodrigues da Silva et al. [51] have explored the decomposition rate of organic residues and the abundance of soil organisms, establishing a direct link between organic residue decomposition and soil organisms' community composition. This finding is relevant to understanding how waste with high TOM levels may interact with soil organisms upon application. Moreover, Wang et al. [52] have demonstrated that compost amendments can enhance soil structure, carbon storage, and microbial biomass. This supports the idea that organic amendments can positively influence soil properties. The pH of the samples is slightly acidic, with a mean value of 6.12, falling within the acceptable range of 6 to 8. However, variations in pH can influence nutrient availability and microbial activity in soil environments. Electrical conductivity (EC) is within the acceptable range at 3151.75 μS/cm, below the recommended limit of 4,000 μS/cm. Elevated EC levels could indicate a high concentration of dissolved salts in the waste, which may affect soil salinity and plant growth if applied as a fertilizer. Total phosphorus (TOP) content is below the recommended limit at 26.92 mg/kg, well below the threshold of 500 mg/kg. Kobierski et al. [53] evaluated the impact of poultry manure fertilization on soil properties, emphasizing the importance of phosphorus levels, which aligns with the need for sufficient TOP. Adequate phosphorus levels are essential for plant growth, and the low TOP content may necessitate supplementation when using poultry manure as a fertilizer. Ca, Mg, K, and Na content are within acceptable ranges, indicating a moderate concentration of these essential nutrients in the poultry manure. Poultry manure has been found to enhance soil nitrogen, phosphorus, organic carbon, calcium, magnesium, and potassium levels compared to mineral fertilizers [54]. This enrichment of soil nutrients can contribute to better plant growth and development. Ammonium concentration is significantly elevated at 2243.75 mg/L, exceeding the recommended limit of below 100 mg/L. However, it has been observed that the concentration of ammonium in poultry manure can sometimes exceed recommended limits, as noted in the statement [55]. High ammonium levels can pose environmental risks such as eutrophication and toxicity to aquatic organisms. Fe, Cu, and Zn contents are within acceptable ranges, indicating moderate concentrations of these metals in the poultry manure.

3.3. RSM for the removal of ammonia from poultry manure

Table 4 presents the Box-Behnken design with actual and predicted values for removing NH_3 from poultry manure using zeolite-A and different ratios of zeolite-A/graphene oxide composite. The factors investigated include stirring time (Factor 1), dosage (Factor 2), and pH (Factor 3), with three different responses (% removal of NH_3) corresponding to three different compositions of zeolite-A/GO (1:1, 2:1, and 1:2). The application of zeolite-A as designated in response 1 revealed the actual and predicted values ranging from 35 to 81 % and 34.25 to 81.75 %, respectively, with optimum removal conditions of stirring time of 45 min, dosage at 5 g and pH of 12 for the removal of NH_3. In response 2, which corresponds to the zeolite-A/GO (1:1) composition, the actual and predicted values for NH_3 removal are provided for each experimental run. The actual removal efficiencies ranged from 33% to 95%, exhibiting optimum values of 30 min, 5 g, and 7 for stirring time, dosage, and pH at 86% NH_3 removal. For response 3, associated with the zeolite-A/GO (2:1) composition, similar experimental conditions were applied with 89% NH_3 removal. Again, the actual removal efficiencies varied across the runs, but the predicted values showed a good agreement with the actual values, indicating the reliability of the model. In response 4, representing the zeolite-A/GO (1:2) composition, the experimental runs exhibited comparable optimum condition trends in NH_3 removal efficiency, exhibiting 95% removal. Despite variations in stirring time, dosage, and pH, the predicted values closely mirrored the actual results, indicating the effectiveness of the model in predicting NH_3 removal under different conditions. The regression analyses were carried out to fit the response functions and determine the removal of NH_3 from poultry manure using nanomaterials, and the obtained regression model equations are as follows Eqns 3-6.

$$\%\ \text{Removal (Response 1)} = 65.40 + 1.50A + 22.63B + 1.13C - 2.25AB - 0.25AC + 1.50BC - 1.45A^2 - 8.20B^2 - 0.70C^2 \quad (3)$$

$$\%\ \text{Removal (Response 2)} = 70.20 + 1.13A + 23.25B + 0.625C - 3.00AB - 0.75AC + 1.00BC - 0.725A^2 - 8.48B^2 - 0.725C^2 \quad (4)$$

Table 4
Box-Behnken design with actual and predicted values for removal of NH_3 from poultry manure using zeolite-A (response 1), zeolite-A/GO (1:1) (response 2), zeolite-A/GO (2:1) (response 3) and zeolite-A/GO (1:2)(response 4).

Run	Factor 1 A:Stirring time (min)	Factor 2 B:Dosage (g)	Factor 3 C:pH	Response 1 Actual	Predicted	Response 2 Actual	Predicted	Response 3 Actual	Predicted	Response 4 Actual	Predicted
1	30	5	7.5	78	79.13	86	86.13	89	89.12	95	95.25
2	60	3	3	62	63.88	69	70.00	73	73.88	78	78.50
3	30	1	7.5	28	29.38	33	33.62	36	36.37	44	44.75
4	45	5	3	77	76.50	83	82.63	87	86.50	92	92.25
5	45	3	7.5	69	65.40	74	70.20	76	73.60	83	78.80
6	45	3	7.5	67	65.40	71	70.20	76	73.60	79	78.80
7	45	1	3	35	34.25	39	38.12	42	41.25	45	44.75
8	30	3	12	65	63.13	70	69.00	72	71.12	78	77.50
9	45	3	7.5	62	65.40	68	70.20	72	73.60	77	78.80
10	45	3	7.5	65	65.40	71	70.20	74	73.60	80	78.80
11	60	1	7.5	38	36.88	42	41.87	46	45.88	50	49.75
12	60	5	7.5	79	77.63	83	82.37	86	85.62	95	94.25
13	45	5	12	81	81.75	85	85.88	87	87.75	93	93.25
14	45	1	12	33	33.50	37	37.37	40	40.50	46	45.75
15	45	3	7.5	64	65.40	67	70.20	70	73.60	75	78.80
16	60	3	12	65	65.63	70	69.75	73	72.63	80	80.50
17	30	3	3	61	60.38	66	66.25	69	69.37	78	77.50

Table 5
ANOVA for quadratic model for zeolite-A.

Source	Sum of Squares	df	Mean Square	F-value	p-value	
Model	4457.29	9	495.25	77.13	< 0.0001	significant
A-Stirring time	18.00	1	18.00	2.80	0.1380	
B-Dosage	4095.13	1	4095.13	637.73	< 0.0001	
C-pH	10.13	1	10.13	1.58	0.2495	
AB	20.25	1	20.25	3.15	0.1190	
AC	0.2500	1	0.2500	0.0389	0.8492	
BC	9.00	1	9.00	1.40	0.2751	
A^2	8.85	1	8.85	1.38	0.2787	
B^2	283.12	1	283.12	44.09	0.0003	
C^2	2.06	1	2.06	0.3213	0.5885	
Residual	44.95	7	6.42			
Lack of Fit	15.75	3	5.25	0.7192	0.5905	not significant
Pure Error	29.20	4	7.30			
Cor Total	4502.24	16				

$R^2 = 0.9900$; Adjusted $R^2 = 0.9772$; Predicted $R^2 = 0.9339$

Table 6
ANOVA for quadratic model for zeolite-A/GO (1:1).

Source	Sum of Squares	df	Mean Square	F-value	p-value	
Model	4694.69	9	521.63	102.71	< 0.0001	significant
A-Stirring time	10.13	1	10.13	1.99	0.2008	
B-Dosage	4324.50	1	4324.50	851.52	< 0.0001	
C-pH	3.13	1	3.13	0.6153	0.4585	
AB	36.00	1	36.00	7.09	0.0324	
AC	2.25	1	2.25	0.4430	0.5270	
BC	4.00	1	4.00	0.7876	0.4043	
A^2	2.21	1	2.21	0.4358	0.5303	
B^2	302.42	1	302.42	59.55	0.0001	
C^2	2.21	1	2.21	0.4358	0.5303	
Residual	35.55	7	5.08			
Lack of Fit	4.75	3	1.58	0.2056	0.8877	not significant
Pure Error	30.80	4	7.70			
Cor Total	4730.24	16				

$R^2 = 0.9925$; Adjusted $R^2 = 0.9828$; Predicted $R^2 = 0.9738$

$$\%\ \text{Removal (Response 3)} = 73.60 + 1.50A + 23.13B + 0.125C - 3.25AB - 0.75AC + 0.50BC - 0.80A^2 - 8.55B^2 - 1.05C^2 \quad (5)$$

$$\%\ \text{Removal (Response 4)} = 78.8 + 1.08A + 23.75B + 0.50C - 1.50AB + 0.50AC + 0.85A^2 - 8.65B^2 - 1.15C^2 \quad (6)$$

Table 5 presents the results of a statistical analysis, and the "Model" row indicates that the overall model is significant, as evidenced by the high F-value (77.13) and the extremely low p-value (< 0.0001). This suggests that at least one of the factors (A, B, C) or their interactions significantly influences the response variable. The "B-Dosage" stands out with a very high F-value (637.73) and an extremely low p-value (< 0.0001), indicating that dosage has a significant effect on the response variable. This is further supported by the large sum of squares (4095.13). However, "A-stirring time" did not appear to have a significant effect, as indicated by its relatively low F-value (2.80) and non-significant p-value (0.1380). Similarly, "C-pH" also seems to have no significant effect based on its F-value (1.58) and p-value (0.2495). Interactions between factors are also examined. For instance, "AB" interaction has a moderately higher F-value (3.15) than AC (0.0389) and BC (1.40) but a non-significant p-value (0.1190), suggesting it may not significantly impact the response variable. The squared terms (A^2 and C^2) show low F-values, while "B^2" has a highly significant F-value (44.09) and low p-value (0.0003), indicating a quadratic effect of dosage, A^2 (1.38) and C^2 (0.3213) did not seem to significantly impact the response variable.

Table 6 presents the results of an Analysis of Variance (ANOVA) for a quadratic model applied to the Zeolite-A/GO (1:1) system. The model itself shows a significant overall fit to the data, as indicated by the highly significant F-value ($F = 102.71$, $p < 0.0001$). This suggests that the model explains a substantial dosage of the variability observed in the response variable. Among the individual factors, dosage (factor B) exhibits a particularly strong effect, with a very high F-value of 851.52 and a highly significant p-value (< 0.0001). This indicates that variations in dosage significantly impact the response variable.

Stirring time (factor A) and pH (factor C) did not appear to have a significant effect, as indicated by its non-significant p-value of 0.2008 and 0.4585, respectively. The interaction term AB shows a significant

Table 7
ANOVA for quadratic model for zeolite-A/GO (2:1).

Source	Sum of Squares	df	Mean Square	F-value	p-value	
Model	4666.58	9	518.51	117.27	< 0.0001	significant
A-Stirring time	18.00	1	18.00	4.07	0.0834	
B-Dosage	4278.13	1	4278.13	967.59	< 0.0001	
C-pH	0.1250	1	0.1250	0.0283	0.8712	
AB	42.25	1	42.25	9.56	0.0175	
AC	2.25	1	2.25	0.5089	0.4987	
BC	1.0000	1	1.0000	0.2262	0.6489	
A^2	2.69	1	2.69	0.6095	0.4606	
B^2	307.80	1	307.80	69.62	< 0.0001	
C^2	4.64	1	4.64	1.05	0.3396	
Residual	30.95	7	4.42			
Lack of Fit	3.75	3	1.25	0.1838	0.9022	not significant
Pure Error	27.20	4	6.80			
Cor Total	4697.53	16				

$R^2 = 0.9934$; Adjusted $R^2 = 0.9849$; Predicted $R^2 = 0.9782$

effect, with a p-value of 0.0324, suggesting that there is a significant interaction between factors A and B. The lack of fit test, with a p-value of 0.8877, indicates that the quadratic model fits the data well, as the lack of fit is not significant. This suggests that the model adequately captures the relationship between the factors and the response variable. The coefficient of determination (R^2) is very high at 0.9925, indicating that the model explains approximately 99.25% of the variability in the response variable. The adjusted R^2 and predicted R^2 values (0.9828 and 0.9738, respectively) also support the adequacy of the model in explaining the variability in the data.

The ANOVA Table 7 for the quadratic model for Zeolite-A/GO (2:1) reveals several noteworthy aspects regarding the removal of NH_3 from poultry manure. Firstly, the model as a whole demonstrates a significant impact on NH_3 removal, as indicated by the highly significant F-value ($F = 117.27$, $p < 0.0001$). This suggests that at least one of the factors or interactions among them has a significant effect on NH_3 removal. Among the individual factors, Dosage (factor B) exhibits an exceptionally high F-value ($F = 967.59$, $p < 0.0001$), indicating its strong influence on NH_3 removal. This suggests that varying the dosage of the Zeolite-A/GO mixture significantly affects the efficiency of NH_3 removal from poultry manure. In contrast, stirring time (factor A) shows a non-significant p-value ($p = 0.0834$), suggesting that it may not have a substantial impact on NH_3 removal at the tested levels. Similarly, the pH (factor C) also displays a non-significant p-value ($p = 0.8712$), indicating that variations in pH levels may not significantly influence NH_3 removal under the conditions studied.

Table 8
ANOVA for quadratic model for zeolite-A/GO (1:2).

Source	Sum of Squares	df	Mean Square	F-value	p-value	
Model	4858.82	9	539.87	96.16	< 0.0001	significant
A-Stirring time	8.00	1	8.00	1.42	0.2715	
B-Dosage	4512.50	1	4512.50	803.75	< 0.0001	
C-pH	2.00	1	2.00	0.3562	0.5694	
AB	9.00	1	9.00	1.60	0.2460	
AC	1.0000	1	1.0000	0.1781	0.6857	
BC	0.0000	1	0.0000	0.0000	1.0000	
A^2	3.04	1	3.04	0.5419	0.4856	
B^2	315.04	1	315.04	56.11	0.0001	
C^2	5.57	1	5.57	0.9918	0.3525	
Residual	39.30	7	5.61			
Lack of Fit	2.50	3	0.8333	0.0906	0.9614	not significant
Pure Error	36.80	4	9.20			
Cor Total	4898.12	16				

$R^2 = 0.9920$; Adjusted $R^2 = 0.9817$; Predicted $R^2 = 0.9801$

The interaction terms AB and BC both exhibit significant p-values ($p = 0.0175$ and $p = 0.6489$, respectively), suggesting that the combined effects of stirring time and dosage, as well as dosage and pH, respectively, have significant impacts on NH_3 removal. The lack of fit test, with a non-significant p-value ($p = 0.9022$), indicates that the quadratic model adequately fits the data, implying that there is no significant difference between the model-predicted values and the actual observed values, thus reinforcing the model's validity. The R-squared value ($R^2 = 0.9934$) indicates that approximately 99.34% of the variability in NH_3 removal can be explained by the model, suggesting an excellent fit. The adjusted R-squared value (Adjusted $R^2 = 0.9849$) and the predicted R-squared value (Predicted $R^2 = 0.9782$) also support the model's reliability and predictability.

In Table 8, the ANOVA results for the quadratic model for Zeolite-A/GO (1:2) reveal several important insights into the removal of NH_3 from poultry manure. The model's F-value of 96.16 with an associated p-value of < 0.0001 indicates that the model is statistically significant, suggesting that at least one of the predictors has a significant effect on NH_3removal. The main effect of parameter B (Dosage) stands out significantly with a high F-value of 803.75 and a very low p-value of < 0.0001. This indicates that the dosage of Zeolite-A/GO has a substantial impact on NH_3 removal, with higher dosages leading to more effective removal.

Parameter A (stirring time) also shows an effect, though it is not statistically significant, as evidenced by its F-value of 1.42 and a p-value of 0.2715. While stirring time may have some influence, it does not appear to be as crucial as dosage in this study. The interactions between parameters (AB, AC, and BC) do not seem to have significant effects, as their associated p-values are all above 0.05, indicating that their combined influence on NH_3 removal is not substantial. Regarding the quadratic terms (A^2, B^2, C^2), only parameter B^2 (dosage) shows a significant effect with a high F-value of 56.11 and a low p-value of 0.0001. This suggests that the quadratic relationship between dosage and NH_3 removal is noteworthy, indicating a non-linear effect of dosage on the removal process. The lack of fit test results further supports the adequacy of the model, as the p-value for lack of fit is 0.9614, indicating that the lack of fit is not significant relative to the pure error. The coefficient of determination (R^2) of 0.9920 suggests that the model explains 99.20% of the variability in NH_3 removal, indicating an excellent fit. The adjusted R^2 and predicted R^2 values also confirm the model's reliability and predictive capability. The plots of contour, 3D response surface, and predicted value against actual values for the removal of NH_3 from poultry manure under the influence of stirring time, dosage, and pH are depicted in Figs. S1–S9.

In this study, the surface area of zeolite-A and graphene oxide directly influences their capacity for NH_3 removal from poultry manure. Zeolite-A, with its high surface area due to its porous structure, provides ample sites for NH_3 adsorption. Graphene oxide, on the other hand, exhibits a large surface area owing to its two-dimensional structure, allowing for effective NH_3 capture. The functional groups present on the surface of zeolite-A and graphene oxide play a crucial role in NH_3 removal. Zeolite-A contains cation exchange sites and hydroxyl groups, facilitating NH_3 adsorption through ion exchange and hydrogen bonding. Graphene oxide possesses oxygen-containing functional groups such as hydroxyl, carboxyl, and epoxide, which can interact with NH_3 molecules through hydrogen bonding and electrostatic interactions. The effect of zeolite-A/graphene oxide dosage on NH_3 removal from poultry manure is significant, and increasing the dosage enhances NH_3 removal due to the increased availability of adsorption sites. Gao et al. [56] demonstrated the significant impact of zeolite dosage on the removal of contaminants, specifically highlighting the

Table 9
The comparison of removal of NH_3 using various adsorbents via Box-Behnken methodology.

Adsorbent	Characterization	Optimum parameter	Removal efficiency	References
Activated Madhuca indica leaves charcoal	TGA, BET, XPS, XRD, FTIR, SEM-EDX	Contact time = 123.19 min, dosage = 29.1 g/L, pH = 10.33, initial ammonia concentration = 312.28 mg/L	100	Bhatlu et al. [59]
Carbon black-sodium dodecyl benzene	SEM, EDX, FTIR, BET, pHpzc	pH = 9, dosage = 5.5 g, Temperature = 30°C, concentration of 0.51 mmol/L	78.78	Mohamed et al. [60]
Coal-based granular activated carbon	SEM, XRD, BET	Contact time = 899.41 min, initial concentration = 17.35 mg/L, Temperature = 15 °C, pH = 6.98	63.74	Yu et al. [61]
Biochar-derived millet shell	SEM, EDS, BET, FTIR, XPS, Zeta potential	Concentration = 310 min, Dosage = 19 g/L, pH = 7, Initial concentration of 50 mg/L	95.07	Chang et al. [62]
Activated carbon from Tamcrid pulp	FTIR	Contact time = 95 min, Dosage = 2 g/100 mL, pH = 11	46.24	NA-Lampang et al. [63]
Zeolite	HRSEM, HRTEM, SAED, EDX mapping, BET, FTIR, XRD	Stirring time = 45 min, Dosage = 5 g, pH = 12, Initial concentration of 2243.75 mg/L	81	This study
Zeolite-A/GO (1:1)	HRSEM, HRTEM, SAED, EDX mapping, BET, FTIR, XRD	Stirring time = 30 min, Dosage = 5 g, pH = 7.5, Initial concentration of 2243.75 mg/L	86	This study
Zeolite-A/GO (2:1)	HRSEM, HRTEM, SAED, EDX mapping, BET, FTIR, XRD	Stirring time = 30 min, Dosage = 5 g, pH = 7.5, Initial concentration of 2243.75 mg/L	89	This study
Zeolite-A/GO (1:2)	HRSEM, HRTEM, SAED, EDX mapping, BET, FTIR, XRD	Stirring time = 30 min, Dosage = 5 g, pH = 7.5, Initial concentration of 2243.75 mg/L	95	This study

enhanced adsorption capacity with increased dosage. Xie et al. [57] reported a 46 % increase in nitrogen removal rates when utilizing graphene oxide at a dosage of 10 mg/L, indicating that higher concentrations of adsorbents correlate with improved pollutant removal. Ergürhan and Erdoğan [58] demonstrated that acid-activated clinoptilolite (a type of zeolite) exhibited NH_3 adsorption capacities ranging from 4.33 to 5.01 mmol/g. Table 9 depicts the summary of previous literature on the removal of NH_3 using adsorbents via Box-Behnken methodology compared to the present study.

3.4. Effect of temperature

The effect of temperature on NH_3 removal using zeolite-A and the composite ratios of zeolite-A/GO was studied for a temperature of 30 to 80 °C at the optimum conditions from RSM (Fig. 9). Fig. 9 shows that a rise in temperature increases the removal percentage of NH_3 in all the samples, and this could be attributed to thermodynamic and kinetic considerations governing the adsorption. The removal efficiencies were relatively low for all the adsorbents at the lowest temperature studied (30 °C), with zeolite A having 45.26% removal and GO-modified composites producing increasingly higher removal with increasing GO content (51.23% for zeolite A/GO (1:1), 52.10% for zeolite A/GO (2:1), and 55.18% for zeolite A/GO (1:2)). The low adsorption capacity at 30 °C indicates that the affinity between NH_3 molecules and the adsorbents is weaker at lower thermal energies, possibly due to lower diffusion rates of NH_3 into the pores of the adsorbents as well as weaker physisorption forces. With the increase in temperature, significant increases in removal efficiencies were observed. The enhancement in NH_3 removal is due to increased molecular mobility and improved diffusion rates at higher temperatures [64,65], which enable the easier migration of NH_3 molecules towards active adsorption sites. Higher temperatures may also reactivate more surface functional groups on the surface of samples, promoting the interaction of NH_3 with the adsorbent surface.

Zeolite A/GO (1:2) exhibits the optimum NH_3 removal efficiency of 92.26% at 80 °C. This suggests the endothermic nature of NH_3 adsorption as a result of an increase in temperature, resulting in enhanced adsorptive capacity. The results from the adsorbents on the removal of NH_3 are temperature-dependent and increase with temperature as a result of better diffusion, increased availability of active sites for adsorption, and enhanced adsorbate-adsorbent interactions. It was established that all the GO-modified zeolites perform higher compared to the pure zeolite A in each case, thus pointing out the synergism with GO addition. From the literature, it has been established that graphene oxide possesses a high concentration of oxygen-functional groups such as hydroxyl, carboxyl, and epoxy groups [66], which could donate their lone pair to establish hydrogen bonding and electrostatic interaction with NH_3 molecules, thus increasing the affinity of the composite for NH_3.

Flory-Huggins model parameters and the Gibbs free energy change (ΔG) in this study were investigated for NH_3 adsorption onto zeolite A and GO-modified composites of zeolite A at different ratios (Table 10). Table 10 presents negative n values typical of the spontaneous adsorption process and represent good interaction between the surface of the adsorbent and adsorbate. The value of n increased with greater GO content in the composite, which corresponds to greater content of GO, making the interaction stronger. The bare zeolite A had the lowest negative n value of -1.287, which supported the enhancement of the adsorption performance on the addition of GO. The adsorbate-adsorbent affinity, as determined by the equilibrium constant K_{FH}, was again maximum in zeolite A/GO (1:2) (1.351) and minimum in zeolite A (1.301). The inclusion of GO improves the adsorption ability, most likely due to its oxygenated functional groups and increased surface area favouring improved NH_3 interaction. The R^2 correlation coefficients for all the samples were > 0.99, confirming a good correlation of the experimental data with the Flory-Huggins model for $_{NH3}$ adsorption behavior for these systems.

One of the most significant thermodynamic parameters of adsorption is the Gibbs free energy change (ΔG), which gives information about the spontaneity and nature of the process. In this study, ΔG was negative and decreased as the temperature increased, indicating that the adsorption of NH_3 is spontaneous and thermodynamically favorable. The increase in the negativity of ΔG with temperature indicates an endothermic adsorption process, where higher thermal energy promotes a higher capacity for adsorption. Of all the materials investigated, zeolite A/GO (1:2) had the most negative ΔG values across the range of temperatures, from -0.7587 kJ/mol at 303 K to -0.8839 kJ/mol at 353 K. This confirms that the most composite with the GO content enhances not just the physical adsorption sites but also adsorbed NH_3 molecules to a higher degree. However, zeolite A possessed the lowest negative ΔG

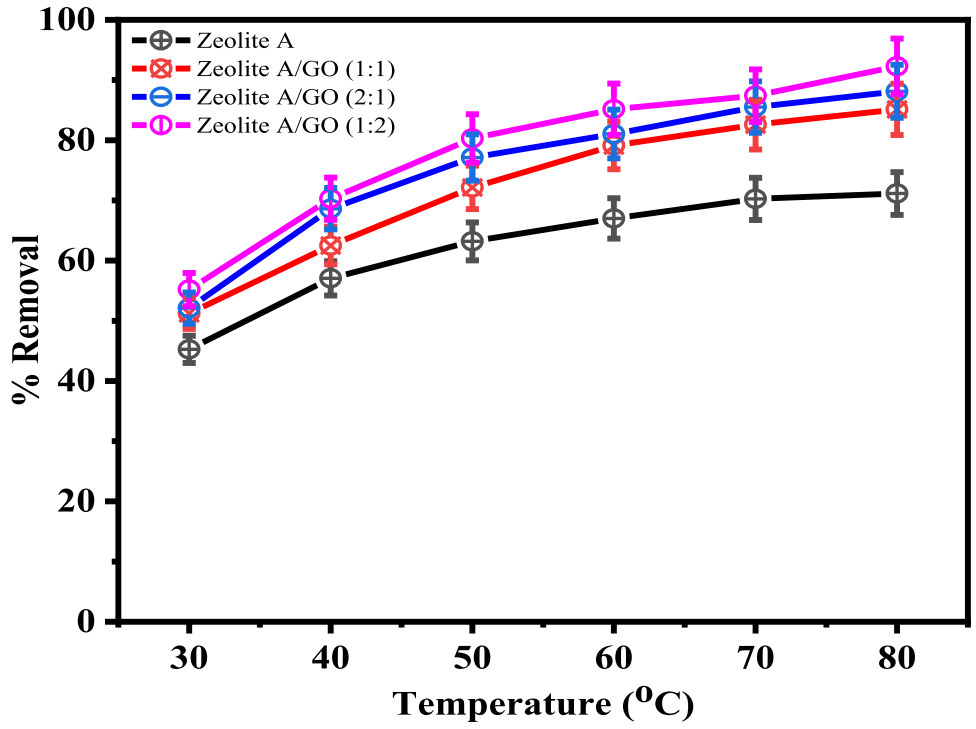

Fig. 9. Effect of temperature for the removal of NH_3 under RSM optimum conditions.

values, ranging from -0.6634 kJ/mol to -0.7729 kJ/mol, as would be expected from its low surface area, lower surface functionality, and pore modification.

3.5. Adsorption mechanism of ammonia removal

The adsorption mechanism of NH_3 removal from poultry manure using a zeolite-A-graphene oxide nanocomposite is based on the synergistic properties of both materials, which enhance the adsorption capacity and efficiency (Fig. 10). Zeolite-A, a microporous aluminosilicate mineral, has a high cation exchange capacity due to its negatively charged framework. This framework allows for the exchange of ammonia ions (NH_4^+) with other cations like sodium (Na^+) within the structure of zeolite. This ion exchange process is a primary mechanism by which zeolite captures and immobilizes ammonia from poultry manure. The porous structure of zeolite provides an extensive surface area for ammonia ions to bind, effectively reducing ammonia levels.

The graphene oxide is a highly functionalized derivative of graphene with oxygen-containing groups such as hydroxyl and carboxyl. These functional groups impart high hydrophilicity and surface reactivity to GO, allowing it to interact with ammonia molecules via hydrogen bonding and electrostatic interactions. The presence of these oxygen functionalities also enhances the adsorption of ammonia by creating additional active sites for binding. The oxygen functional groups present on the GO surface play a crucial role in adsorbing ammonia molecules via hydrogen bonding and electrostatic interactions. NH_3 adsorbed onto GO through π–π interactions between NH_3 molecules and the aromatic rings of the graphene structure.

The zeolite-A-GO exhibits superior performance due to the complementary properties of both materials. The zeolite component contributes to ion exchange and provides a high surface area and strong adsorption affinity for ammonia removal, while the GO enhances surface interaction through physical adsorption and chemisorption mechanisms. The GO component prevents the aggregation of zeolite particles, improving the dispersion of the nanocomposite and increasing the availability of active adsorption sites. Thus, the removal of ammonia using the Zeolite-A-GO nanocomposite occurs via a combination of ion exchange, hydrogen bonding, and electrostatic interactions. Ammonia molecules are initially attracted to the surface of the composite through these interactions, after which they are immobilized within the porous structure of zeolite-A. The high adsorption capacity of nanocomposite is

Table 10
Flory-Huggins model parameters and change in free energy of the removal of NH_3 using zeolite A, zeolite A/GO (1:1), zeolite A/GO (2:1) and zeolite A/GO (1:2).

Adsorbent	Temperature (K)	Flory-Huggins n	K_{FH}	R^2	$\Delta G\left(\frac{kj}{mol}\right)$
Zeolite A/GO (1:2)	303	-1.693	1.351	0.9948	-0.7587
	313				-0.7837
	323				-0.8088
	333				-0.8338
	343				-0.8589
	353				-0.8839
Zeolite A/GO (2:1)	303	-1.415	1.321	0.9943	-0.7007
	313				-0.7238
	323				-0.7470
	333				-0.7701
	343				-0.7932
	353				-0.8163
Zeolite A/GO (1:1)	303	-1.366	1.314	0.9927	-0.6879
	313				-0.7106
	323				-0.7333
	333				-0.7560
	343				-0.7787
	353				-0.8014
Zeolite A	303	-1.287	1.301	0.9930	-0.6634
	313				-0.6853
	323				-0.7072
	333				-0.7291
	343				-0.7510
	353				-0.7729

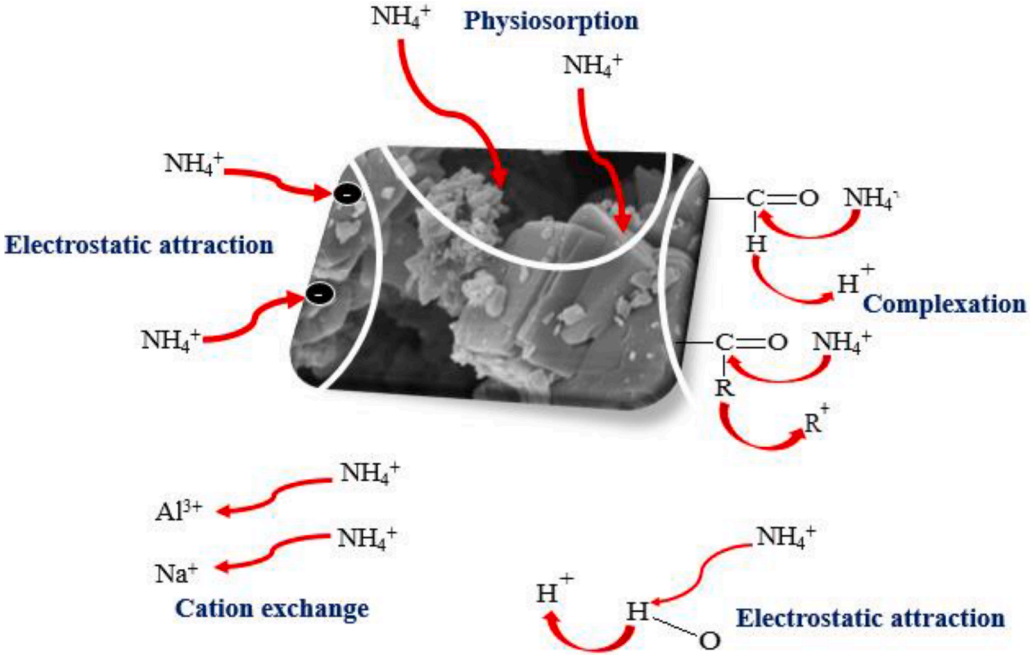

Fig. 10. Proposed mechanism of adsorption of NH_3 using zeolite-A/GO.

attributed to the synergy between the structural stability of zeolite and cation exchange capability and the surface functionalization of GO, which increases the overall surface area and adsorption efficiency. This makes the nanocomposite an effective and efficient material for mitigating ammonia emissions from poultry manure, which otherwise contribute to environmental pollution and odour issues.

3.5.1. Density functional theory of the adsorption mechanism

The HOMO and LUMO distribution demonstrated the enhanced stability and reaction of the nanocomposite with ammonia using DFT calculation The C-Al-N molecule, with 6.615 eV of bandgap, possesses a bandgap, signifying stability and reactivity. The energy of HOMO at -6.769 eV has electron-donating power, while that of LUMO at -0.154 eV is low enough for the acceptance of electrons from ammonia. This electronic configuration allows the interaction with ammonia through charge transfer mechanisms while confirming the stability of the system. Thus, this favours chemisorption pathways. The Na-Al molecule has the smallest bandgap among this series, 2.292 eV, which indicates the highest chemical reactivity among the systems. The low bandgap makes electronic excitation possible, hence promoting ammonia adsorption. The relatively high HOMO energy level of -3.913 eV and the low LUMO energy level of -1.621 eV support a high electron exchange with ammonia molecules, thus favour strong interactions through electrostatic attractions or ion-exchange processes characteristic of zeolite sites. The OH-N structure with a bandgap energy of 9.139 eV has the highest bandgap, equivalent to the most stable but least reactive system. The -6.930 eV HOMO and high-lying LUMO at 2.209 eV limit the electronic transitions necessary for maximum interaction with ammonia. Therefore, this exhibits weak physical adsorption due to the high energy barrier for charge transfer and thus is quite inert towards ammonia. For the Al-N system, the bandgap is 6.327 eV is slightly lower than for the C-Al-N system. This suggests comparable stability, although with slightly higher reactivity. The HOMO energy of -6.996 eV and LUMO of -0.669 eV provide good alignment with interaction with lone pair of ammonia. The negative LUMO also enhances the electron acceptor capability of the system by increasing the tendency for ammonia coordination through Lewis's acid-base interaction.

The C-O-N molecule exhibits an 8.340 eV bandgap, indicating high stability and low reactivity. The LUMO and HOMO at -6.390 eV and 1.950 eV, respectively, suggest a less electronic excitability-prone and poor ammonia adsorption by weak adsorption through physisorption. The positive LUMO also lowers its electron-accepting ability from lone pair ammonia, reducing the chance for strong chemisorption. The Si-N system is characterized by a high bandgap of 7.491 eV, which shows stability but low reactivity. The HOMO lies at -6.854 eV and the LUMO at a moderately positive position of 0.637 eV, indicating poor interaction with ammonia and forces dominated by physisorption as a result of the limited electron-accepting capability of the system and poor conditions for strong chemical forces.

4. Conclusion

The study successfully synthesized and characterized a zeolite-A/graphene oxide nanocomposite for the removal of ammonia from poultry manure, utilizing response surface methodology to optimize the process. A uniform cubic shape zeolite-A, a layered structure for GO, and a unique stacked cubic-spherical morphology for the composite were formed. These observations were supported by analysis confirming covalent bonding between the components. Microscopy image illustrated the effective dispersion of GO on zeolite-A particles, indicating strong interactions. Structural patterns showed orthorhombic structure for zeolite-A with evidence of GO interaction, while functional group identification revealed bonds that facilitate the connection between zeolite-A and GO. The nitrogen adsorption-desorption analysis demonstrated a significant increase in surface area for the zeolite-A/GO composite (69.30 m^2/g) compared to GO (19.35 m^2/g) and zeolite-A (15.88 m^2/g), highlighting the enhancement in adsorption capacity due to the composite's improved surface area. The performance evaluation revealed that the zeolite-A/GO nanocomposite at 1:2 exhibited the highest efficiency removal of 95% from poultry manure compared to zeolite-A alone. The RSM analysis indicated that adsorbent dosage was the most significant factor affecting ammonia removal, followed by stirring time, with pH having the least influence. The quadratic model used in the study provided a strong fit for the data, confirming the effectiveness of the zeolite-A/GO composite in the removal process. The zeolite-A/GO nanocomposite demonstrated substantial potential for enhancing ammonia removal from poultry manure, offering an effective and efficient solution for poultry waste management. The successful

application of response surface methodology further optimized the process parameters, underscoring the composite's superior performance in comparison to individual zeolite-A.

CRediT authorship contribution statement

Jimoh Oladejo Tijani: Writing – original draft, Methodology, Conceptualization. **Muhammad Sani:** Writing – original draft, Conceptualization. **Saheed Mustapha:** Writing – original draft, Conceptualization. **Sarah Udenyi Onogwu:** Writing – review & editing, Supervision, Formal analysis. **Hassana Ladio Abubakar:** Writing – review & editing, Formal analysis. **Ambali Saka Abdulkareem:** Writing – review & editing, Supervision, Funding acquisition, Formal analysis. **Oluwatosin Kudirat Shittu:** Writing – review & editing, Supervision, Formal analysis. **Abdulsalami Sani Kovo:** Writing – review & editing, Supervision, Formal analysis. **Titus Chinedu Egbosiuba:** Writing – review & editing, Supervision, Data curation. **Alechine Emmanuel Ameh:** Writing – review & editing, Supervision, Formal analysis, Data curation. **Muhammed Muhammed Ndamitso:** Writing – review & editing, Supervision, Formal analysis, Data curation. **Ogunmuyiwa O. Enoch:** Writing – review & editing, Formal analysis. **Omar H. Abd-Elkader:** Writing – review & editing, Formal analysis. **Hamad A. Al-Lohedan:** Writing – review & editing, Supervision, Data curation. **Abdelrahman O. Ezzat:** Writing – review & editing, Funding acquisition, Formal analysis, Data curation.

Declaration of competing interest

The authors declare that they have no known competing financial interests or personal relationships that could have appeared to influence the work reported in this paper.

Acknowledgments

The authors acknowledge the financial support through the Ongoing Research Funding program - Research Chairs (ORF-RC-2025-0200), King Saud University, Riyadh, Saudi Arabia. This work was also sponsored and supported by the Tertiary Education Trust Fund, Nigeria (Grant numbers [TETF/DR&D-CE/NRF2020/SETI/116/VOL.1].

Supplementary materials

Supplementary material associated with this article can be found, in the online version, at doi:10.1016/j.materresbull.2025.113672.

Data availability

No data was used for the research described in the article.

References

[1] T.M. Edwards, H.J. Puglis, D.B. Kent, J.L. Durán, L.M. Bradshaw, A.M. Farag, Ammonia and aquatic ecosystems–A review of global sources, biogeochemical cycling, and effects on fish, Sci. Total Environ. (2023) 167911.
[2] R.B. Bist, S. Subedi, L. Chai, X. Yang, Ammonia emissions, impacts, and mitigation strategies for poultry production: a critical review, J. Environ. Manag. 328 (2023) 116919.
[3] C. Hung, N. Hussain, B. Husk, J. Whalen, Ammonia volatilization from manure mixed with biochar, Can. J. Soil Sci. 102 (1) (2022) 177–186.
[4] J. Kim, H. Lee, H.T. Vo, G. Lee, N. Kim, S. Jang, J.B. Joo, Bead-shaped mesoporous alumina adsorbents for adsorption of ammonia, Materials 13 (6) (2020) 1375.
[5] K. Anderson, P. Moore, J. Martin, A. Ashworth, Effect of a new manure amendment on ammonia emissions from poultry litter, Atmosphere 11 (3) (2020) 257.
[6] D. Dróżdż, The influence of poultry manure-derived biochar and compost on soil properties and plant biomass growth, Materials 16 (18) (2023) 6314.
[7] S.M. Muscarella, V.A. Laudicina, B. Cano, L. Badalucco, P. Conte, G. Mannina, Recovering ammonium by treated and untreated zeolitic mixtures: a comprehensive experimental and modelling study, Microporous Mesoporous Mater. 349 (2023) 112434.
[8] G.R. Sallam, H.A. Aly, A.M. Lotfy, M.M. Abdel-Rahim, W.M. Fayed, I.I. Teiba, K. Mzengereza, M. Tembo, W. Singini, Y.J. Habib, A.I. Shehata, Natural zeolite for heavy metal, ammonia removal, and physiological responses in European sea bass (Dicentrarchus labrax) juveniles tanks with different densities, PLoS ONE 19 (4) (2024) e0297844.
[9] T. Taher, E.K.A. Melati, M. Febrina, S. Maulana, M.A. Asagabaldan, A. Rianjanu, A. Lesbani, R.R. Mukti, Effect of desilication on Indonesian natural zeolite for the enhancement of ammonium ion removal from aqueous solutions, Silicon 16 (3) (2024) 1309–1319.
[10] A.J. Kennedy, M.L. Ballentine, A. Das, C.S. Griggs, K. Klaus, M.J. Bortner, Additive manufacturing for contaminants: ammonia removal using 3D printed polymer-zeolite composites, ACS ES&T Water. 13 (2020) 621–629.
[11] N.H. Hieu, Optimization of preparation conditions by response surface methodology for synthesis of titanium dioxide/reduced graphene oxide composite in dye-sensitized solar cells, Mater. Res. Bull. 175 (2024) 112763.
[12] H. Hoseinzadeh, B. Hayati, F.S. Ghaheh, K. Seifpanahi-Shabani, N.M. Mahmoodi, Development of room temperature synthesized and functionalized metal-organic framework/graphene oxide composite and pollutant adsorption ability, Mater. Res. Bull. 142 (2021) 111408.
[13] N. Mushtaq, R. Munir, M. Zia-ur-Rehman, Z. ul-Haq, M.Z. Bashir, A. Muneer, H. Ambreen, S. Noreen, Construction and utilization of innovative zeolite/perovskite/graphene oxide, zeolite/chitosan/graphene oxide, and zeolite/biochar/graphene oxide nanohybrid composites for adsorptive remediation of cationic dye from wastewater, Water Conserv. Sci. Eng. 9 (1) (2024) 33.
[14] A.A. Shati, M.Y. Alfaifi, S.E.I. Elbehairi, B.D. Olegovich, R.H. Althomali, S. S. Abdullaev, E.A.M. Saleh, B.M. Hussien, M.K. Abid, M. Alwave, Functionalization of porous silica with graphene oxide and polyethyleneimine, containing zinc copper ferrite nanoparticles for water treatment and antibacterial application, Environ. Pollut. 348 (2024) 123745.
[15] M.R. Silva, A. Lecus, M. Gajdardziska-Josifovska, M. Schofield, M. Virnoche, J. Chang, J. Chen, D. Garman, Graphene-oxide loading on natural zeolite particles for enhancement of adsorption properties, RSC Adv. 10 (8) (2020) 4589–4597.
[16] Y. Hu, C.Y. Loh, M. Xie, G. Chen, M. Huang, J. Qiao, Ammonia recovery via direct contact membrane distillation: modeling and performance optimization, J. Environ. Manag. 365 (2024) 121683.
[17] N.S. Al-Sailah, B.N. Narayanan, Ag-$NiFe_2O_4$ over mesoporous silica for efficient 4-nitrophenol reduction: nanocatalyst development, kinetics studies and reaction optimization, Mater. Res. Bull. 189 (2025) 113455.
[18] S. Mustapha, M.M. Ndamitso, A.S. Abdulkareem, J.O. Tijani, A.K. Mohammed, D. T. Shuaib, Potential of using kaolin as a natural adsorbent for the removal of pollutants from tannery wastewater, Heliyon 5 (11) (2019).
[19] Y.C. Wang, M.F. Han, T.P. Jia, X.R. Hu, H.Q. Zhu, Z. Tong, Y.T. Lin, C. Wang, D. Z. Liu, Y.Z. Peng, G. Wang, Emissions, measurement, and control of odor in livestock farms: a review, Sci. Total Environ. 1 (2021) 145735.
[20] X. Ren, L. Xiao, R. Qu, S. Liu, D. Ye, H. Song, W. Wu, C. Zheng, X. Wu, X. Gao, Synthesis and characterization of a single-phase zeolite A using coal fly ash, RSC Adv. 8 (73) (2018) 42200–42209.
[21] K.B. Morales, R.I. Hernández, M.B. Liva, E.F. Ledesma, J.A. Rodríguez, F.C. Piñar, Y. Fernández-Afonso, O. Picazo, T. Farías, Low-cost synthesis and characterization of zeolites from silicon natural sources for environmental applications, Acta Microsc. 27 (3) (2018).
[22] Y. Shi, X. Ren, H. Zheng, Y. Zhang, Q. Zuo, Hierarchical 13X zeolite/reduced graphene oxide porous material for trace Pb (II) capturing from drinking water, Microporous Mesoporous Mater. 329 (2022) 111540.
[23] H. Li, X. Liu, S. Qi, L. Xu, G. Shi, Y. Ding, X. Yan, Y. Huang, J. Geng, Graphene oxide facilitates solvent-free synthesis of well-dispersed, faceted zeolite crystals, Angew. Chem. Int. Ed. 56 (45) (2017) 14090–14095.
[24] Z.R. Gao, J. Li, C. Lin, A. Mayoral, J. Sun, M.A. Camblor, HPM-14: a new germanosilicate zeolite with interconnected extra-large pores plus odd-membered and small pores, Angew. Chem. Int. Ed. 60 (7) (2021) 3438–3442.
[25] Z. Qin, G. Melinte, J.P. Gilson, M. Jaber, K. Bozhilov, P. Boullay, S. Mintova, O. Ersen, V. Valtchev, The mosaic structure of zeolite crystals, Angew. Chem. Int. Ed. 128 (48) (2016) 15273–15276.
[26] S.K. Lee, H. Park, J.W. Yoon, K. Kim, S.J. Cho, G. Maurin, R. Ryoo, J.S. Chang, Microporous 3D graphene-like zeolite-templated carbons for preferential adsorption of ethane, ACS Appl. Mater. Interfaces 12 (25) (2020) 28484–28495.
[27] F. Tarannum, R. Muthaiah, S. Danayat, K. Foley, R.S. Annam, K.B. Walters, J. Garg, Chemically edge-carboxylated graphene enhances the thermal conductivity of polyetherimide–graphene nanocomposites, ACS Appl. Mater. Interfaces 14 (12) (2022) 14753–14763.
[28] M.E. Elkartehi, R. Mahmoud, N. Shehata, A. Farghali, S. Gamil, A. Zaher, LDH nanocubes synthesized with zeolite templates and their high performance as adsorbents, Nanomaterials 11 (12) (2021) 3315.
[29] D. Li, L. Qiu, K. Wang, Y. Zeng, T. Williams, Y. Huang, M. Tsapatsis, H. Wang, Growth of zeolite crystals with graphene oxide nanosheets, Chem. Commun. 48 (16) (2012) 2249–2251.
[30] P.V. Viotti, W.M. Moreira, H. Straioto, R. Bergamasco, M.H.N.O. Scaliante, M. F. Vieira, The 'chimie douce'process towards the modification of natural zeolites for removing drugs and pesticides from water, J. Chem. Technol. Biotechnol. 97 (8) (2022) 2149–2162.
[31] Y. Yang, X. Meng, L. Zhu, J. Yang, G. Zhang, H. Shen, X. Cao, Rapid synthesis of Si-rich SSZ-13 zeolite under fluoride-free conditions, Inorg. Chem. 61 (51) (2022) 21115–21122.
[32] P.L.B. Ho, C. Foo, W.C. Lin, S.C.E. Tsang, P.D. Nellist, Spatial differentiation of aluminium siting by the single-atom adsorption sites in zeolite by electron microscopy, Microsc. Microanal. 28 (S1) (2022) 2156–2158.

[33] K. Skrzyńska, G. Cametti, I.O. Galuskina, Y. Vapnik, E. Galuskin, Flörkeite, (K3Ca2Na)[Al8Si8O32]· 12H2O: a rare zeolite from pyrometamorphic rocks of the Hatrurim Complex, Israel, Lithosphere 2022 (1) (2022) 1343791.
[34] T. Triyono, W. Trisunaryanti, I.I. Falah, L. Rahmi, Effect of acetic acid and/or sodium hydroxide treatment towards characters of wonosari natural zeolite for hydrotreatment of castor oil into biofuel, Indones. J. Chem. 23 (2) (2023) 298–308.
[35] M. Naghani, M. Neghabi, M. Zadsar, H. Ahangar, Synthesis and characterization of linear/nonlinear optical properties of graphene oxide and reduced graphene oxide-based zinc oxide nanocomposite, Sci. Rep. 13 (1) (2023).
[36] S. Kanazawa, Y. Yamada, S. Sato, Infrared spectroscopy of graphene nanoribbons and aromatic compounds with sp 3 C–H (methyl or methylene groups), J. Mater. Sci. 56 (2021) 12285–12314.
[37] H. Kim, T. Balgar, E. Hasselbrink, The stretching vibration of hydrogen adsorbed on epitaxial graphene studied by sum-frequency generation spectroscopy, Chem. Phys. Lett. 508 (1-3) (2011) 1–5.
[38] I.A. Popov, K.V. Bozhenko, A.I. Boldyrev, Is graphene aromatic? Nano Research 5 (2012) 117–123.
[39] S. Sakong, P. Kratzer, Hydrogen vibrational modes on graphene and relaxation of the C–H stretch excitation from first-principles calculations, J. Chem. Phys. 133 (5) (2010).
[40] Z. Fatima, A. Afzal, S. Arshad, Tailoring zeolite-composite (ZC) impregnated thermally endured nonporous cellulose acetate membranes for potential gas separation and antibacterial performances, J. Nano Res. 78 (2023) 43–58.
[41] S.U. Rahman, W. Ahmed, N.U. Rehman, M. Alkhedher, E.M. Tag El Din, Fabrication of graphene sheets using an atmospheric pressure thermal plasma jet system, Energies 15 (19) (2022) 7245.
[42] X. Wang, D. Chen, Y. Jia, Z. Jiang, K. Li, S. Chaianansutcharit, P. Reubroycharoen, L. Guo, Preparation of nano-MFI zeolites doped with Al/Ti and their performance in VOC sorption, Dalton Trans. 53 (10) (2024) 4781–4789.
[43] Y. Shi, X. Ren, H. Zheng, Y. Zhang, Q. Zuo, Hierarchical 13X zeolite/reduced graphene oxide porous material for trace Pb (II) capturing from drinking water, Microporous Mesoporous Mater. 329 (2022) 111540.
[44] R. Kukobat, R. Škrbić, P. Massiani, K. Baghdad, F. Launay, M. Sarno, C. Cirillo, A. Senatore, E. Salčin, S.G. Atlagić, Thermal and structural stability of microporous natural clinoptilolite zeolite, Microporous Mesoporous Mater. 341 (2022) 112101.
[45] M. Ulfa, Y.L. Nikmah, Analysis of pores titanium oxide on mesoporous silica-gelatin template using nitrogen adsorption by BET, BJH and t-plot methode, in: Proceedings of the AIP Conference 2645, AIP Publishing, 2022.
[46] M.R. Silva, A. Lecus, M. Gajdardziska-Josifovska, M. Schofield, M. Virnoche, J. Chang, J. Chen, D. Garman, Graphene-oxide loading on natural zeolite particles for enhancement of adsorption properties, in: RSC Adv., 10, 2020, pp. 4589–4597.
[47] A. Chaturvedi, P.P. Kundu, Co-doped zeolite–GO nanocomposite as a high-performance ORR catalyst for sustainable bioelectricity generation in air-cathode single-chambered microbial fuel cells, ACS Appl. Mater. Interfaces 14 (29) (2022) 33219–33233.
[48] World Health Organization, Guidelines for the Safe Use of Wastewater, Excreta and Greywater, Volume II,, World Health Organization, Paris, France, 2006, p. 182.
[49] E.J. Falodun, R. Egharevba, Influence of poultry manure rates and spacing on growth, yield, nutrient concentration, uptake and proximate composition of onion (Allium cepa L.), Not. Sci. Biol. 10 (1) (2018) 117–123.
[50] H. He, M. Peng, Z. Hou, J. Li, Unlike chemical fertilizer reduction, organic fertilizer substitution increases soil organic carbon stock and soil fertility in wheat fields, J. Sci. Food Agric. 104 (5) (2024) 2798–2808.
[51] L.J. Rodrigues da Silva, T.A. Feitosa de Souza, L. Klestadt Laurindo, H. Freitas, M. C. Costa Campos, Decomposition rate of organic residues and soil organisms' abundance in a Subtropical Pyrus pyrifolia field, Agronomy 12 (2) (2022) 263.
[52] D. Wang, J.Y. Lin, J.M. Sayre, R. Schmidt, S.J. Fonte, J.L. Rodrigues, K.M. Scow, Compost amendment maintains soil structure and carbon storage by increasing available carbon and microbial biomass in agricultural soil–a six-year field study, Geoderma 427 (2022) 116117.
[53] M. Kobierski, A. Bartkowiak, J. Lemanowicz, M. Piekarczyk, Impact of poultry manure fertilization on chemical and biochemical properties of soils, Plant Soil Environ. 63 (12) (2017) 558.
[54] J.O. Adegoke, O.O. Oyekanmi, B.T. Alabi, O.A. Hassan, Influence of manures on some soil fertility properties, yield and agronomic efficiencies of soybean (Glycine max) on degraded acid soil, J. Exp. Agric. Int. 45 (7) (2023) 42–49.
[55] S.O. Ogaji, A.O. Watako, J.M. Nyongesah, B. Peter, Effects of cricket frass biofertilizer on growth of spring onion (Allium fistulosum L.) and physicochemical properties of soil, J. Mod. Agric. Biotechnol. 1 (3) (2022) 14.
[56] M. Gao, L. Yang, S. Yang, T. Jiang, F. Wu, T. Nagasaka, Simple aminated modified zeolite 4A synthesized using fly ash and its remediation of mercury contamination: characteristics and mechanism, Sustainability 14 (23) (2022) 15924.
[57] Y. Xie, C. Zou, S. Ismail, L. Xie, S.Q. Ni, Dosage-dependent impacts of graphene oxide on the anammox process: performance and mechanism. ACS ES&T Eng., 2024.
[58] O. Ergürhan, B. Erdoğan, Structural and ammonia adsorption properties of the gördes clinoptilolite after HCl acid treatment, Gazi Univ. J. Sci. (2024).
[59] L.D. Bhatlu M, P. Ray, P. Biswal, B. Sahoo, C. Nayak, Eco-friendly ammonia adsorption from aqueous solutions using activated madhuca indica leaves charcoal and optimization of parameters by RSM-BBD: a sustainable zero-waste approach, Langmuir (2025).
[60] N.B. Mohamed, N. Ngadi, N.Y. Yahya, M.H. Mohamed Noor, A.A. Bakar, N. Ali, Optimization study of ammonium adsorption from aqueous solution on carbon black modified with sodium dodecylbenzene sulfonate: kinetics, isotherms, and thermodynamics, Arab. J. Sci. Eng. (2025) 1–22.
[61] A. Yu, Y. Liu, X. Li, Y. Yang, Z. Zhou, H. Liu, Modeling and optimizing of NH_4^+ removal from stormwater by coal-based granular activated carbon using RSM and ANN coupled with GA, Water 13 (5) (2021) 608.
[62] H. Chang, X.Y. Yang, D. Liang, Z.Q. Chen, X. Liu, Enhanced removal of ammonium nitrogen from aqueous solutions using a novel biochar derived from millet shells through both static adsorption and dynamic column experiments, J. Water Process Eng. 58 (2024) 104848.
[63] C. NA-Lampang, P. Assawasaengrat, L. Phumjan, W. Narkrugsa, P. Sriprom, Optimizing ammonia adsorption using activated carbon from tamarind pulp, J. Jpn. Inst. Energy 100 (12) (2021) 288–293.
[64] D. Rana, B.M. Mandal, S.N. Bhattacharyya, Miscibility and phase diagrams of poly (phenyl acrylate) and poly (styrene-co-acrylonitrile) blends, Polymer 34 (7) (1993) 1454–1459.
[65] D. Rana, B.M. Mandal, S.N. Bhattacharyya, Analogue calorimetry of polymer blends: poly (styrene-co-acrylonitrile) and poly (phenyl acrylate) or poly (vinyl benzoate), Polymer 37 (12) (1996) 2439–2443.
[66] N. Kumari, M. Bhandari, Surface Functionalization Reactions of Graphene-Based Nanostructure and Their Practical Application, IntechOpen, 2024. Published: 22 May 2024.